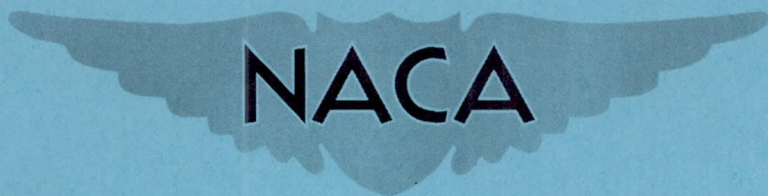


CONFIDENTIAL

Copy
RM L50C24

221

NACA RM L50C24



RESEARCH MEMORANDUM

AN INVESTIGATION OF A SUPERSONIC AIRCRAFT CONFIGURATION
HAVING A TAPERED WING WITH CIRCULAR-ARC
SECTIONS AND 40° SWEEPBACK

A PRESSURE-DISTRIBUTION STUDY OF THE AERODYNAMIC
CHARACTERISTICS OF THE WING AT
MACH NUMBER 1.59

By Morton Cooper and M. Leroy Spearman

Langley Aeronautical Laboratory
Langley Air Force Base, Va.

CLASSIFIED DOCUMENT

This document contains classified information affecting the National Defense of the United States within the meaning of the Espionage Act, USC 50:31 and 32. Its transmission or the revelation of its contents in any manner to an unauthorized person is prohibited by law. Information so classified may be imparted only to persons in the military and naval services of the United States, appropriate civilian officers and employees of the Federal Government who have a legitimate interest therein, and to United States citizens of known loyalty and discretion who of necessity must be informed thereof.

CLASSIFICATION CHANGED TO UNCLASSIFIED
AUTHORITY: NACA RESEARCH ABSTRACT NO. 128
DATE: JUNE 24, 1958

WHL

NATIONAL ADVISORY COMMITTEE FOR AERONAUTICS

WASHINGTON
May 23, 1950

CONFIDENTIAL

NATIONAL ADVISORY COMMITTEE FOR AERONAUTICS

RESEARCH MEMORANDUM

AN INVESTIGATION OF A SUPERSONIC AIRCRAFT CONFIGURATION

HAVING A TAPERED WING WITH CIRCULAR-ARC

SECTIONS AND 40° SWEEPBACK

A PRESSURE-DISTRIBUTION STUDY OF THE AERODYNAMIC

CHARACTERISTICS OF THE WING AT

MACH NUMBER 1.59

By Morton Cooper and M. Leroy Spearman

SUMMARY

A pressure-distribution investigation of the wing (in the presence of the fuselage) of a complete supersonic aircraft configuration has been conducted in the Langley 4- by 4-foot supersonic tunnel at a Mach number of 1.59 and a Reynolds number of 0.575×10^6 based on the mean aerodynamic chord. The wing was swept back 40° and had an aspect ratio of 4, a taper ratio of 0.5, and 10-percent-thick circular-arc sections perpendicular to the quarter-chord line. For the Mach number of the present investigation, the wing had both supersonic leading and trailing edges; the leading edge, however, had a detached shock wave throughout the angle-of-attack range.

The experimental lift and drag coefficients were less than those predicted by linear theory. The discrepancies resulted principally from the existence of large regions of separated flow at the rear and at the outboard stations of the wing and in part from the presence of a detached leading-edge shock which is neglected in the linear theory. In addition, there was a pronounced interference effect of the fuselage on the wing at the inboard stations but this effect diminished fairly rapidly outboard.

The maximum lift-drag ratio of 5.3 obtained experimentally agreed very well with the theoretical value of 5.1. This agreement, however, was partially the result of compensating discrepancies in both the lift

and drag coefficients. The pitching moment was considerably less stable than predicted by theory primarily as a result of the separation over the outboard region of the wing. This separation phenomenon appears to be of primary concern for uncambered and untwisted swept wings, such as the wing of the present investigation, where the spanwise gradients and their effects on the boundary layer are large.

INTRODUCTION

A comprehensive investigation of a supersonic aircraft configuration having a tapered wing with circular-arc sections, aspect ratio 4, and 40° sweepback has been conducted in the Langley 4- by 4-foot supersonic tunnel. In order to obtain a detailed knowledge of the flow over the model as well as to determine the general aerodynamic characteristics, extensive tests were conducted on both a large-scale force and pressure model of the complete configuration and of various components at Mach numbers of 1.40 and 1.59. The results of the pressure-distribution study of the fuselage and its canopies are reported in reference 1 for a Mach number of 1.59 and in reference 2 for a Mach number of 1.40. The first phase of the force-model investigation, which evaluated the static longitudinal stability and control characteristics at a Mach number of 1.40, has been reported in reference 3.

The present report presents the results of the pressure-distribution study of the wing obtained during tests of the complete pressure model at a Mach number of 1.59 and a Reynolds number of 0.575×10^6 based on the mean aerodynamic chord. For this Mach number, the wing had both supersonic leading and trailing edges; the leading edge, however, had a detached shock wave throughout the angle-of-attack range. The pressure data have been analyzed in terms of section and over-all wing characteristics, and the experimental results have been compared throughout the paper with linear theoretical calculations to evaluate differences between the theory and experiment.

SYMBOLS

Free-stream conditions:

ρ	mass density of air
V	airspeed
a	speed of sound in air

M Mach number (V/a)

q dynamic pressure $\left(\frac{1}{2}\rho V^2\right)$

p static pressure

Wing geometry:

S area extended through the fuselage

b span

A aspect ratio (b^2/S)

c airfoil chord at any spanwise station

c' mean aerodynamic chord $\left(\frac{2}{S} \int_0^{b/2} c^2 dy\right)$

\bar{c} mean chord (S/b)

x chordwise distance measured streamwise from the airfoil leading edge

y spanwise distance measured from the plane of symmetry of the wing

z normal distance measured from the airfoil chord line

α angle of attack of the wing, degrees

Pressure data:

p_l local static pressure

P pressure coefficient $\left(\frac{p_l - p}{q}\right)$

c_n section normal-force coefficient $\left(\int_0^1 (P_L - P_U) d(x/c)\right)$

- c_c section chord-force coefficient $\left(\int_0^1 \left[\left(P \frac{dz}{dx} \right)_U - \left(P \frac{dz}{dx} \right)_L \right] d \left(\frac{x}{c} \right) \right)$
- c_l section lift coefficient $(c_n \cos \alpha - c_c \sin \alpha)$
- c_d section pressure-drag coefficient $(c_n \sin \alpha + c_c \cos \alpha)$
- c_m section pitching-moment coefficient, due to normal forces, about the 25-percent position of the airfoil chord $\left(\int_0^1 (P_L - P_U) \left(0.25 - \frac{x}{c} \right) d \left(\frac{x}{c} \right) \right)$
- $c_{m_{x_1}}$ section pitching-moment coefficient, due to normal forces, about a line perpendicular to the plane of symmetry and passing through the 25-percent position of the mean aerodynamic chord $\left(\int_0^1 (P_L - P_U) \left(\frac{x_1}{c} - \frac{x}{c} \right) d \left(\frac{x}{c} \right) \right)$
- x_1 distance from the leading edge of each spanwise station to a line perpendicular to the plane of symmetry and passing through the 25-percent position of mean aerodynamic chord (positive rearward from leading edge)
- C_L wing lift coefficient $\left(C_L = \int_0^1 c_l \frac{c}{c'} d \left(\frac{y}{b/2} \right) = \frac{\text{Lift}}{qS} \right)$
- C_D wing drag coefficient $\left(C_D = \int_0^1 c_d \frac{c}{c'} d \left(\frac{y}{b/2} \right) = \frac{\text{Drag}}{qS} \right)$
- C_m wing pitching-moment coefficient about a line perpendicular to the plane of symmetry and passing through the 25-percent position of the mean aerodynamic chord $\left(C_m = \frac{\bar{c}}{c'} \int_0^1 \frac{c_{m_{x_1}} c^2}{\bar{c}^2} d \left(\frac{y}{b/2} \right) = \frac{\text{Pitching moment}}{qS \bar{c}'} \right)$

$\frac{y_{cp}}{b/2}$

spanwise location of the center of pressure of the normal

$$\text{force} \left(\int_0^1 \frac{c_{nc}}{c} \frac{y}{b/2} d\left(\frac{y}{b/2}\right) \middle/ \int_0^1 \frac{c_{nc}}{c} d\left(\frac{y}{b/2}\right) \right)$$

 n_o

chordwise location of the wing aerodynamic center

$$\left(0.25 - \frac{\partial C_m}{\partial C_L} \right)$$

Subscripts:

- L' lower surface
 U upper surface
 α value at angle of attack
 $\alpha = 0$ value at 0° angle of attack

APPARATUS

Tunnel.- The Langley 4- by 4-foot supersonic tunnel is a rectangular, closed-throat, single-return wind tunnel designed for a nominal Mach number range from 1.2 to 2.2. The test section Mach number is varied by deflecting horizontal flexible walls against a series of fixed interchangeable templates which have been designed to produce uniform flow in the test section. For the present investigation, the nozzle walls were set for a test section Mach number of 1.59. For this Mach number, the test section has a width of 4.5 feet and a height of 4.4 feet. A detailed description of the tunnel, together with the calibration data of the test section at this Mach number, is presented in reference 1.

Model.- The test model, shown in figure 1 prior to installation in the tunnel, was constructed to the dimensions shown in figure 2. The complete model contained a total of 254 orifices which were located on the wing, fuselage, and horizontal tail surfaces. During the tests, pressures were measured simultaneously over the entire model. As pointed out in the introduction, however, this paper will be concerned only with the wing of the configuration and will deal with other components of the model only insofar as they affect the flow over the wing.

The wing was constructed with a steel core and has steel leading and trailing edges. The wing surface between approximately the 10-percent and 98-percent chordwise location was made of bismuth and tin. The geometry of the wing is as follows:

Span, feet	2.155
Area extended through the fuselage, square feet	1.158
Mean chord, feet	0.537
Mean aerodynamic chord, feet	0.557
Aspect ratio (wing extended to fuselage center line)	4
Sweepback of quarter-chord line, degrees	40
Taper ratio	0.5
Airfoil sections	Symmetrical circular arcs in planes perpendicular to the quarter-chord line
Thickness ratio:	
Section perpendicular to quarter-chord line, percent	10
Section parallel to air-stream direction, percent	8
Location of maximum thickness:	
Section perpendicular to quarter-chord line, percent	50
Section parallel to air-stream direction, percent	52.1
Geometric twist, degrees	0
Dihedral of quarter-chord line in a plane normal to the chord plane, degrees	3

The left semispan of the model contained 116 orifices divided approximately equally among each of four streamwise stations. The locations of the streamwise stations (shown in fig. 3 and indicated in fig. 1 by the white lines on the left wing) at 18.6, 43.6, 68.6, and 93.7 percent of the wing semispan were selected to present a representative picture of the flow over the wing. In addition to these orifices, two rows of orifices (figs. 1 and 3), containing a total of 30 orifices, were located at two oblique stations perpendicular to the quarter-chord line of the right wing semispan.

The wing was mounted on a fuselage which consisted of a body of revolution, upon which upper- and lower-surface canopies (fig. 2) were installed. The fuselage has a length of 2.522 feet and a fineness ratio of 9.4 without canopies. A complete description of the fuselage, together with coordinates, is presented in reference 1. The wing was set at a fixed incidence of 3° relative to the fuselage axis. Since this paper presents primarily wing data, the angle of attack has been referenced to the wing chord line; hence, a given angle of attack is indicated as being 3° higher than the corresponding angle in references 1 to 3.

During all the tests, the model was frequently inspected and polished in an attempt to maintain an aerodynamically smooth surface.

Installation.- The model was sting supported with the wing in a vertical plane as shown in figure 4. The angle of attack was varied through fixed increments by rotating the model about the 59-percent position of the fuselage. This axial location corresponds to the 0.25-chord position of the mean aerodynamic chord. The pressure tubes from the orifices were brought out from the wing through the fuselage and the sting to multiple-tube manometers.

TESTS

The basic pressure data over the wing were obtained for an angle-of-attack range from -2° to 13° at a Mach number of 1.59 and a Reynolds number of 575,000 based on the mean aerodynamic chord. The aerodynamic data have been obtained at tunnel stagnation conditions of: pressure, 0.25 atmosphere; temperature, 110° F; and dew point, -35° F. For these test conditions, the calibration data (reference 1) of the test section indicate that the effects of condensation on the flow over the model are probably extremely small.

CORRECTIONS AND ACCURACY

Since the magnitudes of the flow angle, Mach number, and pressure gradients are small in the vicinity of the model, no corrections due to these sources have been applied to the data. Furthermore, from optical measurements obtained during these tests, it was found that the wing twist under load was negligible, amounting to less than 0.05° for all angles of attack. Consequently, no corrections for twist have been applied.

It is estimated that the accuracy of the wing data is as follows:

Stream Mach number	± 0.01
Angle of attack:	
Geometric measurement (probable error), degree	± 0.02
Maximum flow irregularity, degree	± 0.10
Absolute value of pressure coefficient	± 0.010

PRESENTATION OF RESULTS

The basic pressure data for the wing, obtained during tests of the complete model, are presented for the four streamwise and two oblique

stations in figures 5 and 6, respectively, for angles of attack of -2° , 0° , 1° , 3° , 5° , 7° , 9° , 11° , and 13° . In these figures, as in all other figures, flagged symbols have been used to designate the lower-surface data. In order to facilitate the use of these data for other purposes, the numerical values of all the pressure data plotted in figures 5 and 6 are tabulated in tables I and II. In addition to the pressure distributions (presented in figs. 5 and 6) which are indicative of the normal loads, the distribution of chordwise load is presented in figure 7 for the streamwise stations for representative angles of attack of -2° , 0° , 5° , and 13° . In this figure, the unit chord-force coefficient at each position along the chord has been defined as the product of the local pressure coefficient and the local slope in the streamwise direction.

The pressure data of figure 5 are compared with linear theoretical calculations for 0° angle of attack in figure 8 and for angle of attack in figure 9. The theoretical calculations for 0° were obtained by the method of reference 4 as applied in reference 5. In obtaining the theoretical curves for angle of attack (fig. 9), the method of reference 6 was used for stations 0.186, 0.436, and 0.686; for station 0.937 the method of reference 7 which accounts for the tip effect was used in addition to reference 6. In the calculation of the theoretical wing pressures, the fuselage side was assumed to impose a physical reflection plane, and, as such, was arbitrarily selected as the origin of calculations. In figure 9, detailed data have been presented for station 0.436. Since the other stations exhibit similar trends, only representative data have been included for stations 0.186, 0.686, and 0.937. Since the theoretical surface lifting-pressure coefficient per unit angle of attack for a given station is equal for both surfaces, these data (fig. 9) could have been compared against a single theoretical curve for each station. However, inasmuch as a fundamental purpose of this investigation has been to evaluate differences between theory and experiment, the experimental data have been separated into expansion and compression surfaces by defining the surface lifting-pressure coefficient as
$$\frac{57.3 (P_\alpha - P_{\alpha=0})}{|\alpha|}$$
. In this way, the upper surface at a positive angle of attack and the lower surface at a negative angle of attack are considered equivalent.

The section normal-force, chord-force, and pitching-moment coefficients at the four spanwise stations have been obtained by integrating the pressure data of figures 5 and 7 and are presented in figure 10. The section lift and drag coefficients, also presented in this figure, were obtained from a resolution of the normal- and chord-force coefficients. In each case, the coefficients presented in figure 10 have been compared with the results obtained from linear theory. Since the drag coefficients were obtained from integrated pressure data, the direct effects of skin friction are not included; and therefore the experimental

drag coefficients are on a comparable basis with the theoretical drag calculations. These same data have been presented in figures 11, 12, and 13 to show the spanwise distribution of the section coefficient and load parameters for normal force, drag, and pitching moment. In these figures, only one theoretical curve has been shown for reference purposes. The theoretical curves for other conditions can be obtained from figure 10. For the pitching-moment data of figure 13, the coefficients have been referenced to the quarter-chord line of the individual sections while the loading parameters have been referenced to a line which is perpendicular to the plane of symmetry of the model and passes through the 25-percent position of the mean aerodynamic chord. Figure 14, which has been derived from figures 11 and 13, presents a comparison of the experimental and theoretical locations of the centers of pressure of the normal forces at each spanwise station.

The over-all wing characteristics, obtained from integration of the spanwise distributions, are presented in figure 15 as a function of the wing angle of attack. In this presentation, the experimental and theoretical curves were obtained by extrapolating the data from the wing-fuselage junction to the center line of the model. This method, therefore, leads to coefficients which are more equivalent to a wing-alone configuration than to a wing-body combination. For application of these results to wing-body combinations, the primary change would occur in the pitching-moment coefficient (fig. 15) which would be more stable than indicated in this paper since the lift carry-over region in the presence of a fuselage would be farther rearward (references 8, 9, and 10). Figure 16 presents the experimental and theoretical wing lift-drag ratios (obtained from fig. 15) and compares these results with the lift-drag ratios obtained during force tests of the complete model and of the wing-fuselage combination (unpublished data). Figure 17 presents a comparison of the experimental and theoretical location of the lateral center of pressure $\frac{y_{cp}}{b/2}$, and the aerodynamic center n_o to indicate quantitatively the accuracy with which the root bending moments and the margin of static stability of the wing can be predicted.

DISCUSSION

Limitations of experimental and theoretical comparison.- In the analysis of the experimental results, the data have been compared throughout the paper with linear theoretical calculations to indicate the accuracy with which the wing characteristics can be estimated at the present time. In interpreting this comparison, it must be fully appreciated that the application of theoretical calculations for an

isolated wing to the wing of a complete model entails fundamental assumptions in addition to those inherent in the linear theory. The combined effect of these additional approximations, the neglecting of the fuselage flow field together with the nose cone and canopy shocks, will in part be evident. Another, and perhaps more important, limitation on the theoretical-experimental comparison involves the shock-detachment phenomenon. For the present combination of Mach number, sweep angle, and leading-edge angle of the airfoil section, the shock wave at the wing leading edge is detached for all angles of attack including the 0° condition. Thus, though the leading edge is supersonic in the usual sense (the ratio of the cotangent of the sweep angle to the tangent of the Mach angle is 1.34), this detached shock leads to a small region of subsonic flow in the immediate vicinity of the leading edge, a phenomenon which will be apparent in the data and which violates a fundamental assumption of the linear theory. Thus the comparison of the present paper will provide some additional information on the practical importance of this latter limitation.

Section Pressure Characteristics

Shock-detachment phenomena.- The pressure data (figs. 5 and 6) immediately reflect the influence of the detached shock wave in the vicinity of the leading edge. The pressure peak at the nose of the airfoil is particularly evident for stations 0.186 and 0.436 at 5° angle of attack and for stations 0.686 and 0.937 at 3° angle of attack or higher. This pressure peak is characteristic of flow around sharp corners at subsonic speeds and would not occur if the leading-edge shock waves were attached. This phenomenon has been previously reported in reference 11 for sharp-nose airfoils at high subsonic speeds. The gradual compression shown behind this peak at all the stations indicates a very small separated region followed by an oblique shock (reference 11). Even at the highest angles of attack where the angle of attack is larger than the half-angle of the leading edge of the airfoil, the significant effects of the subsonic flow region on the leading edge of the upper surface can be seen, particularly for station 0.186.

Wing-body interference.- The effect of the presence of the body on the wing pressure data can be seen clearly for zero angle of attack from figure 8. These data show that, for the root section, the upper-surface pressures are more positive than the lower-surface pressures; this effect diminishes fairly rapidly outboard. Attempts to predict the magnitude of the discrepancy between the upper- and lower-surface pressure distributions by superposing the fuselage flow field on the wing field were inadequate, principally because of the mixed nature of the flow in this

vicinity of the wing. A similar effect of the body on the wing can be observed at angles of attack (fig. 5) by noting that the angle of attack for the leading-edge pressure peaks is lower at the outboard stations.

It should be noted that the primary body interference effect upon the flow over the wing for this configuration is restricted to gradual changes rather than the discrete and finite disturbances which might have been anticipated. From an examination of unpublished schlieren photographs taken at a Mach number of 1.55 in the Langley 9-inch supersonic tunnel during tests of a small-scale model of the same configuration (reference 12), it is clearly evident that the shock wave from the nose and canopies did not cross the wing to produce any discontinuous disturbances up to angles of attack of 5° (the limit of tests in reference 12). Since there are no unexpected regions of rapidly increasing pressure at the higher angles of attack, it is quite probable that the wing was clear of the nose and canopy shock for the complete range of angles of attack of the investigation.

The extremely rapid increase in pressure indicated by the last orifice on station 0.186 (fig. 5) and, to a lesser extent, on station A (fig. 6) appears to be caused by a fuselage interference effect.

Separation effects.- The experimental data for zero angle of attack (fig. 8) show surprisingly good agreement with the theoretical calculations for the inboard station, 0.186, with progressively poorer agreement outboard. Since the effects of the fuselage diminish fairly rapidly outboard, the discrepancies in the outboard region must result mainly from the approximations of the linear wing theory. Hence, the better agreement inboard may be taken as indicative of the fact that the mutual wing-fuselage interference effects occurring inboard appear to compensate, in part, in the present application for the approximations in the wing theory.

The data of figure 8 also show, for zero angle of attack, a progressive build-up of laminar separation from about the rear 15 percent of the chord at the root to about the rear 30 percent of the chord at the tip. This separation occurs in spite of an apparent favorable chordwise pressure gradient upon the boundary layer. However, the effect of the rapid increase in pressure caused by the shock wave at the wing trailing edge is transmitted upstream through the boundary layer and induces separation. This trailing-edge-separation phenomenon occurs for all angles of attack (figs. 5 and 6). It exists on the upper surface to a small degree for negative angles of attack, and increases progressively as the angle of attack is increased (trailing-edge shock is increased). The reverse occurrence, as would be expected, exists for the lower surface. This phenomenon of boundary-layer separation induced by the trailing-edge shock has been noted many times previously and is discussed, for example, in reference 13. The greater extent of the separation at the outer

stations is attributed to the spanwise flow which increases the boundary-layer thickness at the outboard stations. At the highest angles of attack there appear to be large regions of essentially zero pressure change with chordwise position. Theoretically, however, there is a continually decreasing chordwise pressure except in the immediate vicinity of the Mach line (for example, about 25 percent of the chord at station 0.436). Hence, these regions of no pressure change seem to indicate completely separated flow. In considering this problem, it should be noted that the linear theory, when applied even to estimate the pressures at these high angles, predicts that a vacuum ($P = -0.565$) exists at the trailing edge of station 0.436 for an angle of attack of 13° . Hence an absolute physical limit to the theory is reached at this point; a more realistic limit, however, occurs at a much lower angle of attack.

Lifting pressures.- The experimental lifting-pressure data of figure 9 indicate, in general, that the expansion surface produces slightly more lift than the compression surface. This effect appears to be directly related to the subsonic nature of the flow at the immediate vicinity of the leading edge and the associated pressure peaks. In this figure, as in figure 8, the root section again appears to give the best agreement with theory. Because of the detached shock coupled with the interference and viscous effects, the large pressure variations in the vicinity of the root and tip Mach lines are not present. Insofar as the tip section is concerned, the effects of the detached shock at the leading edge, together with laminar boundary-layer separation farther rearward, completely dominate the flow field. From an over-all examination of the data of figure 9 some idea of the degree of non-linearity of the problem of computing the flow over comparable wing installations having similar flow fields can be gained. If the lowest angles (-2° to 3°) are neglected because of the limitations on the precision of the surface lifting pressures in this range, there appear to be only small regions for which the flow varies linearly with angle of attack. At the leading- and trailing-edge portions of the chord, subsonic flow and viscous effects, respectively, appear to invalidate any linear considerations of the problem.

Section Characteristics

From a general consideration of the effects of the leading-edge subsonic region and the laminar separation at the rear and outboard stations, as shown in figures 5, 6, and 9, it would be expected that the section drag would be reduced and the pitching moment would become less stable than predicted theoretically. The section lift would be expected to decrease if the loss in lift resulting from the separation phenomena outweighs the effects of the pressure peaks caused by the detached flow at the leading edge. Of course, these considerations are

necessarily limited by the fact that only linear considerations were used to obtain the theoretical curves. In general, figure 10 verifies these trends in the section characteristics; the lower lift coefficients for the four stations indicate the predominance of the boundary-layer separation as compared to the leading-edge subsonic flow region. Both the section drag coefficients and the stability (as indicated by the slope of the pitching-moment-coefficient curve) are less than predicted in all cases. It can also be seen that the chord-force coefficient is less than the theoretical value due to the laminar separation but that the coefficient is relatively constant, as predicted. In general, the section drag coefficients (fig. 10) for stations 0.436, 0.686, and 0.937 indicate reasonably close agreement with each other. The drag coefficients for station 0.186, however, are lower for the same angle of attack. This is probably, in part, a result of interference of the fuselage on the wing. If the drags for the individual stations are compared on the basis of the same lift, the agreement between the inboard station and the outboard stations is improved, indicating that the interference effect is primarily a downwash caused by the fuselage. In addition, since the minimum drag coefficients at the inboard stations are less than those of the outboard stations, there may also be a slight horizontal bouyancy effect of the pressure field of the body on the root sections.

Spanwise Characteristics

The experimental span-load curves of figure 11 reflect the same overestimation of the lift that was indicated in figure 10. In addition, the experimental center of pressure of the normal forces is farther inboard than predicted by theory by approximately 4 percent of the wing semispan as shown in figure 17. From structural considerations, this latter effect will result in too conservative an estimate of the wing bending moments.

Both the pitching-moment-coefficient and the pitching-moment-parameter curves presented in figure 13 indicate the inadequacy of the theory for predicting either the pitching moment on the wing or the wing twisting moment for structural purposes. The linear theory predicts too negative a pitching-moment coefficient throughout the wing semispan. On the other hand, the theoretical pitching-moment parameter, which determines the over-all wing pitching moment, is too negative for approximately the outboard two-thirds of the wing semispan and agrees relatively well for the remainder of the wing. This inboard agreement, however, is coincidental since it results from compensating discrepancies in both the magnitude (fig. 11) and location (fig. 14) of the section normal forces in this region.

In addition to affecting the pitching moments, the fact that the experimental centers of pressure are forward of the theoretical locations (fig. 14) will have a slight effect on the downwash. On the basis of the theory of reference 14, it is estimated that this effect will be small, amounting to an overestimation of the downwash by about 4 percent for the present configuration.

Over-All Wing Characteristics

In comparing the over-all wing lift and drag coefficients, figure 15, it can be seen that both the wing lift and drag are lower than the theoretical values. The experimental lift-curve slope is about 0.044 as compared to a theoretical value of 0.053. This reduction in lift is believed to be primarily an effect of the laminar separation from the rear and the outboard part of the wing. The minimum drag coefficient is about 0.023 compared to a theoretical value of 0.030; the comparison in both cases is based on pressure drag. The experimental drag-rise factor $\Delta C_D / \Delta C_L^2$ is approximately 0.366 (based on C_L values of -0.016 and 0.3), compared to 0.329 (the reciprocal of the theoretical lift-curve slope) as given by theory. This indicates a higher rate of increase of drag with lift coefficient than predicted by theory. If the experimental lift-curve slope were used in estimating the drag-rise factor, then the value would be 0.397. This indicates that the actual drag-rise factor is slightly more favorable than the value obtained from superposition with the assumption that the chord force is independent of the angle of attack. In comparing experimental and theoretical drag-rise factors, it should be noted that the experimental value depends significantly upon the two lift coefficients used since the experimental drag curve is not a true parabola as assumed.

The pitching-moment comparison of figure 15 for the complete wing clearly indicates the overestimation of the pitching moment that was foreshadowed in figure 13. As previously noted, this discrepancy results primarily from the inability to predict the flow over the outboard two-thirds of the wing semispan because of the large amounts of separated flow in this vicinity. In general, the magnitude of the pitching-moment coefficient is fairly large, resulting in a high static margin of stability, as can be seen from the aerodynamic-center location (fig. 17).¹ These high values of the stability of the wing have resulted in a limitation of the trim lift coefficient of the complete configuration (unpublished data) to a value of 0.35.

¹For this consideration, the center of gravity has been assumed to be located at 25 percent of the mean aerodynamic chord to satisfy low-speed stability requirements.

The general comparison of the lift and drag has indicated experimental values less than theoretical values for a given angle of attack. Hence a comparison of these coefficients on the basis of equal lift would show much better agreement. This is essentially the result shown in figure 16 where the agreement between the experimental and theoretical lift-drag ratios is quite good. The maximum L/D of 5.3 obtained experimentally and 5.1 obtained theoretically serve to indicate the low lift-drag ratios which will result for the complete configuration. Even these values are somewhat idealized since they represent wing-alone characteristics with the effects of skin friction neglected. To illustrate this point, force characteristics obtained from as yet unpublished data for the complete model and for the wing and body are presented to show the results to be expected from more complete configurations of this model. The difference between the experimental wing and wing-body lift-drag ratios represents a difference in drag coefficient of approximately 0.019 in the range of low lift coefficients. This value of 0.019 must therefore account for the body and part of the wing-body interference drag together with the skin-friction drag of the wing. Since the body drag alone was approximately 0.013, it appears that the skin-friction drag of the wing is low, tending to substantiate the assumption that the flow in the boundary layer over the wing is almost completely laminar. It appears, therefore, that the low maximum lift-drag ratios are primarily associated with a combination of thick wing sections (8 percent in the streamwise direction) and inadequate sweep for this Mach number.

From the viewpoint of improving the maximum lift-drag ratio, if maximum lift-drag ratio is of primary interest at this Mach number, the principal opportunity appears to be in increasing the sweep angle to a value of about 65° with corresponding reductions in section thicknesses consistent with structural limitations. (See references 15 and 16.) It also appears that in order to minimize the adverse spanwise flow effects which might seriously hamper and reduce the lateral control effectiveness, the use of a cambered wing would materially improve the flow.

CONCLUDING REMARKS

A pressure-distribution investigation of the wing (in the presence of the fuselage) of a complete supersonic aircraft configuration has been conducted in the Langley 4- by 4-foot supersonic tunnel at a Mach number of 1.59 and a Reynolds number of 0.575×10^6 based on the mean aerodynamic chord. The wing was swept back 40° and had an aspect ratio of 4, a taper ratio of 0.5, and 10-percent-thick circular-arc sections perpendicular to the quarter-chord line. For the Mach number of the present investigation, the wing had both supersonic leading and trailing edges; the leading edge, however, had a detached shock wave throughout the angle-of-attack range.

The experimental lift and drag coefficients were less than those predicted by linear theory. The discrepancies resulted principally from the existence of large regions of separated flow at the rear and at the outboard stations of the wing and in part from the presence of a detached leading-edge shock which is neglected in the linear theory. In addition, there was a pronounced interference effect of the fuselage on the wing at the inboard stations but this effect diminished fairly rapidly outboard.

The maximum lift-drag ratio of 5.3 obtained experimentally agreed very well with the theoretical value of 5.1. This agreement, however, was materially aided by compensating discrepancies in both the lift and drag coefficients. The pitching moment was considerably less stable than predicted by theory primarily as a result of the separation over the outboard region of the wing. This separation phenomenon appears to be of primary concern for uncambered and untwisted swept wings, such as the wing of the present investigation, where the spanwise gradients and their effects on the boundary layer are large.

Langley Aeronautical Laboratory
National Advisory Committee for Aeronautics
Langley Air Force Base, Va.

REFERENCES

1. Cooper, Morton, Smith, Norman F., and Kainer, Julian H.: A Pressure-Distribution Investigation of a Supersonic Aircraft Fuselage and Calibration of the Mach Number 1.59 Nozzle of the Langley 4- by 4-Foot Supersonic Tunnel. NACA RM L9E27a, 1949.
2. Hasel, Lowell E., and Sinclair, Archibald R.: A Pressure-Distribution Investigation of a Supersonic-Aircraft Fuselage and Calibration of the Mach Number 1.40 Nozzle of the Langley 4- by 4-Foot Supersonic Tunnel. NACA RM L50B14a, 1950.
3. Spearman, M. Leroy: An Investigation of a Supersonic Aircraft Configuration Having a Tapered Wing with Circular-Arc Sections and 40° Sweepback. Static Longitudinal Stability and Control Characteristics at a Mach Number of 1.40. NACA RM L9L08, 1950.
4. Jones, Robert T.: Thin Oblique Airfoils at Supersonic Speed. NACA Rep. 851, 1946.
5. Kainer, Julian H.: Theoretical Calculations of the Supersonic Pressure Distribution and Wave Drag for a Limited Family of Tapered Sweptback Wings with Symmetrical Parabolic-Arc Sections at Zero Lift. NACA TN 2009, 1949.
6. Puckett, Allen E.: Supersonic Wave Drag of Thin Airfoils. Jour. Aero. Sci., vol. 13, no. 9, Sept. 1946, pp. 475-484.
7. Evvard, John C.: Distribution of Wave Drag and Lift in the Vicinity of Wing Tips at Supersonic Speeds. NACA TN 1382, 1947.
8. Ferrari, Carlo: Interference between Wing and Body at Supersonic Speeds - Theory and Numerical Application. Jour. Aero. Sci., vol. 15, no. 6, June 1948, pp. 317-336.
9. Ferrari, Carlo: Interference between Wing and Body at Supersonic Speeds - Note on Wind-Tunnel Results and Addendum to Calculations. Jour. Aero. Sci., vol. 16, no. 9, Sept. 1949, pp. 542-546.
10. Ellis, Macon C., Jr., and Grigsby, Carl E.: Aerodynamic Investigation at Mach Number 1.92 of a Rectangular Wing and Tail and Body Configuration and Its Components. NACA RM L9L28a, 1950.
11. Lindsey, W. F., Daley, Bernard N., and Humphreys, Milton D.: The Flow and Force Characteristics of Supersonic Airfoils at High Subsonic Speeds. NACA TN 1211, 1947.

12. Ellis, Macon C., Jr., Hasel, Lowell E., and Grigsby, Carl E.:
Supersonic-Tunnel Tests of Two Supersonic Airplane Model Configurations. NACA RM L7J15, 1947.
13. Ferri, Antonio: Elements of Aerodynamics of Supersonic Flows. The MacMillan Co., 1949, pp. 143-154.
14. Mirels, Harold, and Haefeli, Rudolf C.: Line-Vortex Theory for Calculation of Supersonic Downwash. NACA TN 1925, 1949.
15. Jones, Robert T.: Estimated Lift-Drag Ratios at Supersonic Speeds. NACA TN 1350, 1947.
16. Madden, Robert T.: Aerodynamic Study of a Wing-Fuselage Combination Employing a Wing Swept Back 63° . - Investigation at a Mach Number of 1.53 to Determine the Effects of Cambering and Twisting the Wing for Uniform Load at a Lift Coefficient of 0.25. NACA RM A9C07, 1949.

TABLE I.- PRESSURE-COEFFICIENT DATA FOR
FOUR STREAMWISE STATIONS

$$(a) \frac{y}{b/2} = 0.186$$

Percent chord upper surface	Pressure coefficient, P, for angle of attack of -								
	-2°	0°	1°	3°	5°	7°	9°	11°	13°
1.020	0.508	0.411	0.340	0.166	-0.023	-0.205	-0.301	-0.326	-0.375
2.549	.403	.321	.282	.139	.034	-.132	-.242	-.299	-.367
4.971	.341	.271	.241	.114	.036	-.085	-.200	-.271	-.340
7.521	.283	.222	.200	.098	.026	-.068	-.182	-.256	-.318
9.943	.259	.201	.178	.088	.020	-.054	-.165	-.234	-.300
11.727	.242	.175	.167	.076	.010	-.053	-.153	-.216	-.290
13.512	.213	.152	.128	.059	-.003	-.065	-.153	-.191	-.277
19.885	.135	.090	.055	.004	-.047	-.103	-.151	-.202	-.257
25.876	.085	.041	.007	-.047	-.096	-.150	-.194	-.224	-.277
40.790	.015	-.009	-.050	-.111	-.149	-.195	-.240	-.260	-.310
50.988	-.018	-.043	-.077	-.131	-.175	-.212	-.252	-.277	-.322
60.293	-.043	-.051	-.091	-.148	-.175	-.220	-.277	-.269	-.314
72.020	-.102	-.101	-.136	-.189	-.210	-.248	-.277	-.281	-.324
82.473	-.142	-.136	-.171	-.221	-.230	-.269	-.291	-.293	-.328
89.484	-.169	-.128	-.151	-.199	-.200	-.265	-.299	-.293	-.328
97.132	-.171	-.120	-.144	-.184	-.198	-.244	-.223	-.212	-.251
Percent chord lower surface									
2.040	0.071	0.201	0.243	0.327	0.399	0.461	0.517	0.571	0.614
6.119	.069	.155	.174	.241	.298	.353	.404	.457	.509
11.090	.032	.105	.116	.174	.223	.275	.331	.390	.444
18.228	.001	.068	.079	.131	.176	.230	.284	.337	.383
23.072	-.014	.051	.059	.106	.152	.198	.247	.297	.346
29.955	-.145	.016	.018	.065	.107	.148	.193	.252	.321
46.526	-.088	-.041	-.044	-.006	.034	.079	.127	.183	.241
55.959	-.125	-.057	-.064	-.029	.014	.058	.107	.156	.205
66.794	-.146	-.082	-.089	-.049	-.011	.026	.070	.118	.164
76.864	-.175	-.112	-.122	-.090	-.058	-.023	.016	.063	.102
84.895	-.204	-.141	-.151	-.125	-.092	-.060	-.025	.020	.059
91.396	-.169	-.136	-.159	-.146	-.114	-.089	-.050	-.008	.030
97.387	-.179	-.128	-.157	-.172	-.149	-.122	-.075	-.041	-.002

CONFIDENTIAL

NACA RM L50C24

CONFIDENTIAL

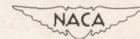
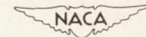


TABLE I.- PRESSURE-COEFFICIENT DATA FOR
FOUR STREAMWISE STATIONS - CONTINUED

$$(b) \frac{y}{b/2} = 0.436.$$

Percent chord upper surface	Pressure coefficient, P, for angle of attack of -								
	-2°	0°	1°	3°	5°	7°	9°	11°	13°
5.477	0.376	0.290	0.243	0.131	-0.040	-0.160	-0.256	-0.283	-0.350
20.429	.213	.155	.128	.061	.003	-.109	-.198	-.242	-.310
26.351	.151	.101	.071	.014	-.032	-.117	-.207	-.252	-.314
30.348	.102	.040	.028	-.058	-.087	-.146	-.223	-.269	-.322
33.309	.073	-.016	-.001	-.103	-.123	-.173	-.231	-.279	-.328
40.266	.027	-.047	-.044	-.137	-.158	-.197	-.248	-.293	-.338
46.780	-.010	-.055	-.077	-.158	-.165	-.212	-.264	-.289	-.350
51.369	-.034	-.097	-.085	-.195	-.203	-.248	-.264	-.305	-.346
60.992	-.076	-.097	-.128	-.213	-.203	-.261	-.285	-.297	-.362
67.358	-.092	-.143	-.132	-.234	-.237	-.285	-.291	-.297	-.350
77.276	-.138	-.141	-.177	-.215	-.235	-.273	-.310	-.297	-.354
85.270	-.179	-.159	-.183	-.213	-.217	-.261	-.293	-.273	-.350
90.007	-.200	-.130	-.165	-.217	-.201	-.238	-.272	-.271	-.334
97.557	-.208		-.151				-.268		-.326
Percent chord lower surface									
3.553	0.153	0.296	0.340	0.413	0.482	0.545	0.601	0.652	0.699
7.254	.139	.230	.266	.335	.402	.467	.525	.579	.632
11.695	.096	.184	.221	.282	.347	.406	.461	.516	.565
34.493	-.051	.026	.038	.073	.125	.173	.226	.276	.334
42.783	-.092	-.014	-.003	.023	.074	.118	.171	.223	.282
48.409	-.117	-.045	-.034	-.008	.040	.083	.136	.195	.245
55.366	-.146	-.070	-.066	-.045	.001	.044	.094	.154	.201
63.360	-.177	-.101	-.099	-.076	-.034	.005	.061	.114	.156
71.799	-.208	-.128	-.128	-.119	-.070	-.032	.016	.065	.105
86.751	-.224	-.155	-.185	-.184	-.133	-.101	-.066	-.023	.016
92.228	-.208	-.136	-.165	-.201	-.152	-.128	-.093	-.049	-.016
96.817	-.200	-.134	-.157	-.213	-.172	-.156	-.120	-.080	-.046



CONFIDENTIAL

CONFIDENTIAL

NACA RM L50C24

TABLE I.- PRESSURE-COEFFICIENT DATA FOR
FOUR STREAMWISE STATIONS - CONTINUED

$$(c) \frac{v}{v/2} = 0.686$$

Percent chord upper surface	Pressure coefficient, P, for angle of attack of -								
	-2°	0°	1°	3°	5°	7°	9°	11°	13°
2.476	0.488	0.390	0.286	0.016	-0.151	-0.259	-0.295	-0.328	-0.387
4.775	.420	.319	.262	.112	-.096	-.207	-.233	-.317	-.383
10.080	.337	.265	.221	.114	-.037	-.150	-.217	-.265	-.330
20.159	.230	.167	.135	.061	-.037	-.140	-.227	-.254	-.318
33.245	.112	.065	.038	-.027	-.072	-.167	-.260	-.252	-.302
39.965	.054	.013	-.017	-.076	-.108	-.205	-.277	-.281	-.334
46.508	.013	-.020	-.050	-.111	-.135	-.214	-.289	-.287	-.336
50.928	-.014	-.047	-.077	-.133	-.157	-.232	-.293	-.289	-.348
55.880	-.034	-.059	-.087	-.156	-.167	-.227	-.318	-.297	-.342
66.844	-.094	-.113	-.144	-.204	-.212	-.269	-.299	-.307	-.338
72.325	-.123	-.122	-.155	-.227	-.218	-.257	-.291	-.289	-.324
79.929	-.162	-.170	-.190	-.260	-.216	-.242	-.285	-.293	-.326
84.881	-.187	-.147	-.155	-.258	-.198	-.236	-.281	-.283	-.322
90.186	-.204	-.122	-.140	-.236	-.190	-.234	-.281	-.277	-.310
97.259	-.181	-.126	-.142	-.219	-.194	-.228		-.271	-.314
Percent chord lower surface									
2.476	0.166	0.315	0.377	0.473	0.550	0.609	0.661	0.709	0.748
7.427	.135	.246	.291	.366	.442	.493	.550	.536	.648
11.848	.116	.207	.243	.311	.379	.410	.482	.484	.584
16.446	.094	.190	.213	.262	.330	.380	.426	.351	.533
30.062	.003	.068	.092	.137	.198	.249	.296	.305	.403
36.428	-.034	.030	.048	.094	.154	.200	.247	.256	.355
42.971	-.072	-.001	.012	.045	.109	.153	.197	.219	.308
48.806	-.101	-.039	-.021	.012	.070	.116	.160	.191	.265
53.581	-.121	-.045	-.038	-.017	.046	.085	.131	.158	.235
58.179	-.146	-.078	-.071	-.043	.014	.054	.098	.120	.203
63.837	-.171	-.103	-.097	-.076	-.019	.022	.063	.087	.168
69.850	-.198	-.134	-.128	-.107	-.051	-.013	.030	.044	.130
76.923	-.214	-.145	-.149	-.141	-.084	-.052	-.005	-.012	.087
87.533	-.181	-.143	-.175	-.189	-.129	-.101	-.060	-.037	.024
93.015	-.179	-.134	-.159	-.205	-.147	-.122	-.083	-.082	-.016
97.436	-.179	-.136	-.153	-.225	-.177	-.156	-.126		-.055

CONFIDENTIAL

NACA RM L50C24

CONFIDENTIAL

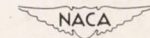


TABLE I.- PRESSURE-COEFFICIENT DATA FOR
FOUR STREAMWISE STATIONS - CONCLUDED

(a) $\frac{y}{b/2} = 0.937$

Percent chord upper surface	Pressure coefficient, P, for angle of attack of -								
	-2°	0°	1°	3°	5°	7°	9°	11°	13°
2.420	0.506	0.382	0.299	-0.002	-0.171	-0.269	-0.343	-0.348	-0.407
9.901	.345	.265	.217	.102	-.068	-.169	-.248	-.323	-.350
13.641	.296	.219	.176	.086	-.064	-.164	-.240	-.277	-.342
20.242	.234	.074	.044	.057	-.043	-.142	-.202	-.224	-.283
30.363	.122	.074	.040	-.010	-.092	-.171	-.240	-.273	-.330
33.223	.089	.032	.005	-.025	-.088	-.167	-.227	-.250	-.308
36.744	.052	.011	-.013	-.013	-.104	-.179	-.240	-.263	-.319
40.264	.023	-.030	-.052	-.066	-.112	-.183	-.240	-.263	-.316
46.865	-.016	-.109	-.134	-.098	-.139	-.201	-.244	-.277	-.318
67.327	-.123	-.138	-.161	-.182	-.192	-.254	-.297	-.299	-.342
77.228	-.171	-.126	-.142	-.223	-.216	-.273	-.318	-.309	-.350
85.369	-.198	-.118	-.132	-.242	-.218	-.275	-.322	-.313	-.356
92.629	-.179		-.136	-.201	-.198	-.242	-.318	-.291	-.350
98.350	-.162				-.190		-.291		-.342
Percent chord lower surface									
2.860	0.106	0.313	0.375	0.468	0.538	0.594	0.638	0.687	0.727
7.701	.151	.294	.334	.399	.473	.525	.573	.622	.665
12.321	.135	.232	.268	.336	.402	.455	.502	.557	.604
16.722	.110	.190	.225	.286	.353	.406	.453	.508	.557
23.322	.069	.140	.167	.219	.282	.332	.381	.435	.484
28.383	.027	.095	.112	.157	.217	.267	.313	.370	.413
31.903	.007	.070	.085	.119	.180	.226	.272	.327	.371
35.424	-.018	.032	.046	.078	.135	.181	.222	.278	.322
38.504	-.034	.024	.032	.053	.109	.150	.193	.248	.290
43.564	-.059	-.012	-.005	.012	.064	.101	.144	.195	.233
49.505	-.080	-.030	-.034	-.025	.020	.054	.092	.142	.180
56.326	-.123	-.076	-.071	-.068	-.025	.005	.041	.089	.124
64.466	-.154	-.084	-.093	-.107	-.064	-.048	-.013	.034	.065
88.009	-.167	-.118	-.144	-.209	-.171	-.167	-.143	-.104	-.079
93.729	-.165	-.113	-.134	-.221	-.185	-.183	-.165	-.126	-.105
98.350	-.162	-.126	-.142	-.201	-.198	-.220	-.215	-.181	-.168

CONFIDENTIAL

CONFIDENTIAL

NACA RM L50C24

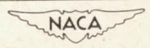
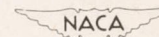


TABLE II.- PRESSURE-COEFFICIENT DATA

FOR TWO OBLIQUE STATIONS

(a) Station A

Percent chord upper surface	Pressure coefficient, P, for angle of attack of -								
	-2°	0°	1°	3°	5°	7°	9°	11°	13°
2.273	0.451	0.371	0.295	0.102	-0.104	-0.226	-0.295	-0.303	-0.354
8.902	.327	.263	.196	.111	-.039	-.146	-.235	-.285	-.346
29.545	.104	.072	.026	-.025	-.080	-.169	-.237	-.277	-.330
36.364	.048	.018	-.025	-.072	-.118	-.189	-.260	-.291	-.344
63.068	-.109	-.116	-.159	-.211	-.242	-.281	-.310	-.334	-.385
80.114	-.175	-.161	-.188	-.244	-.271	-.302	-.328	-.326	-.369
93.939	-.212	-.147	-.167	-.193	-.226	-.246	-.256	-.258	-.314
Percent chord lower surface									
4.356	0.160	0.284	0.321	0.417	0.481	0.541	0.597	0.648	0.693
22.727	.011	.099	.108	.164	.209	.263	.313	.370	.423
46.591	-.117	-.086	-.093	-.004	.050	.081	.131	.191	.241
56.250	-.171	-.132	-.151	-.064	-.023	.018	.070	.126	.172
73.295	-.216	-.143	-.188	-.144	-.096	-.056	-.013	.032	.075
87.879	-.191	-.132	-.157	-.180	-.143	-.115	-.077	-.033	.002
96.402	-.187			-.240	-.175	-.156	-.120	-.082	-.042



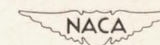
CONFIDENTIAL

CONFIDENTIAL

TABLE II.- PRESSURE-COEFFICIENT DATA FOR TWO
OBLIQUE STATIONS - CONCLUDED

(b) Station B

Percent chord upper surface	Pressure coefficient, P, for angle of attack of -								
	-2°	0°	1°	3°	5°	7°	9°	11°	13°
12.077	0.306	0.246	0.190	0.116	-0.064	-0.162	-0.240	-0.281	-0.344
23.188	.176	.134	.087	.024	-.084	-.175	-.240	-.281	-.336
36.473	.075	.047	.001	-.053	-.125	-.205	-.266	-.285	-.338
47.101	.003	-.014	-.058	-.109	-.153	-.236	-.291	-.307	-.356
63.043	-.088	-.093	-.138	-.184	-.214	-.260	-.303	-.297	-.332
73.671	-.142	-.134	-.175	-.225	-.242	-.252	-.285	-.293	-.332
82.609	-.187	-.153	-.163	-.266	-.224	-.248	-.285	-.297	-.336
94.203	-.190	-.164	-.168	-.255	-.227	-.257	-.292	-.311	-.348
Percent chord lower surface									
2.174	0.177	0.337	0.409	0.503	0.570	0.626	0.679	0.721	0.761
8.937	.143	.237	.279	.350	.412	.468	.525	.575	.627
17.633	.079	.150	.186	.246	.303	.357	.413	.463	.518
29.710	-.012	.057	.084	.135	.189	.239	.294	.245	.397
56.522	-.157	-.107	-.086	-.044	.002	.045	.093	.143	.193
68.599	-.209	-.169	-.149	-.111	-.070	-.031	.017	.063	.108
80.193	-.177	-.197	-.194	-.165	-.124	-.089	-.040	.002	.043
93.961	-.172	-.159	-.167	-.219	-.184	-.150	-.107	-.068	-.027



CONFIDENTIAL

CONFIDENTIAL

NACA RM L50C24

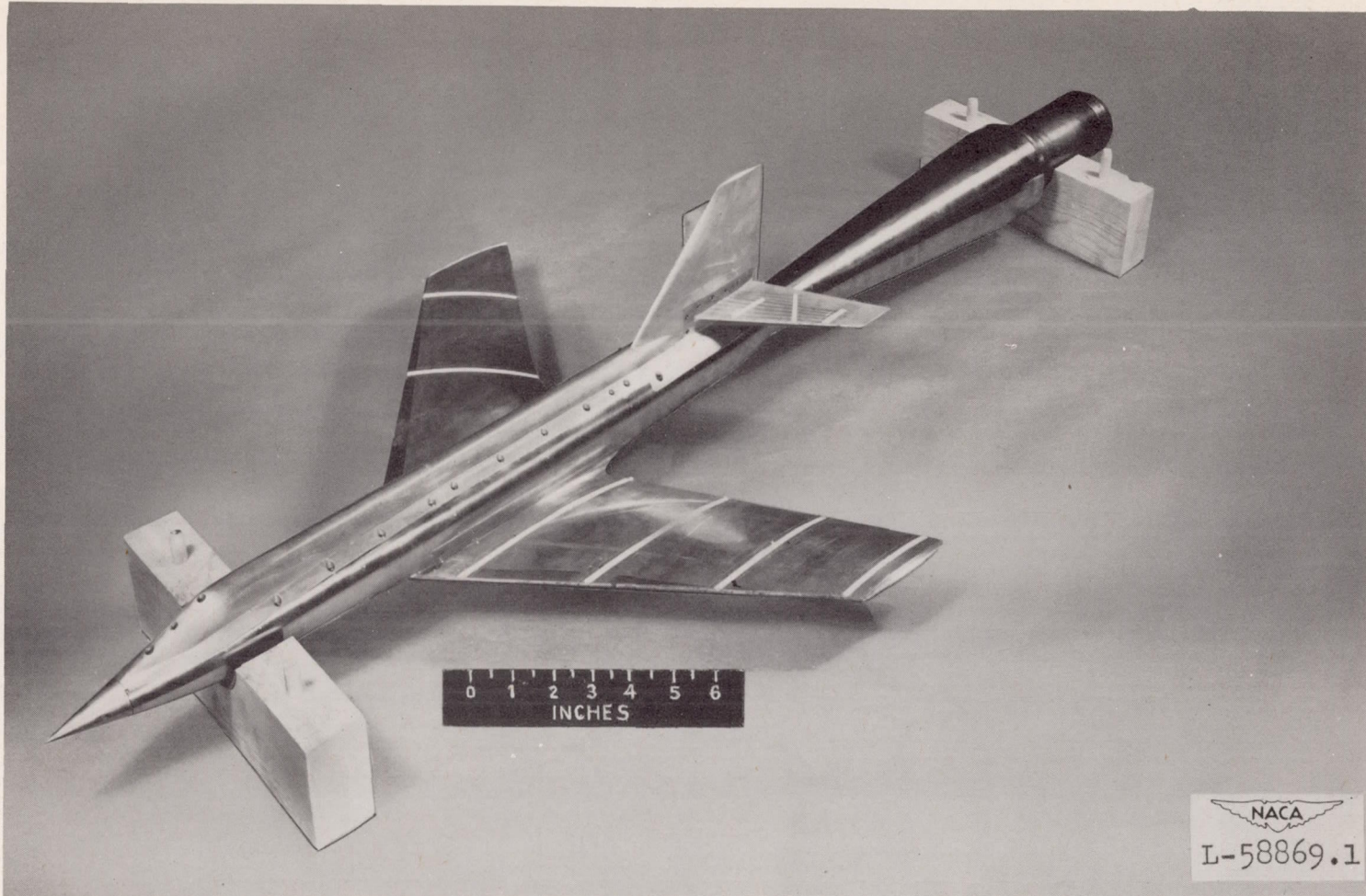
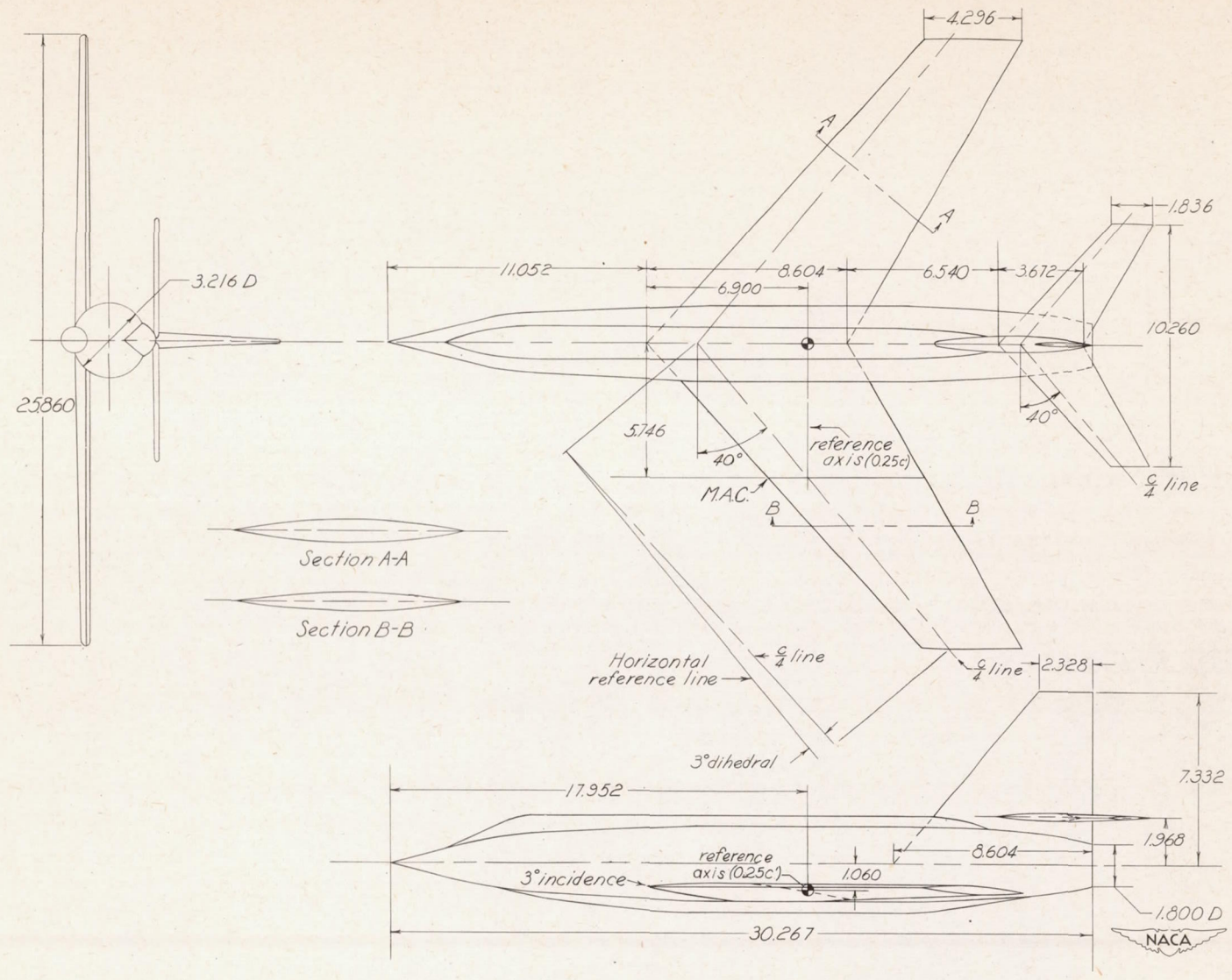


Figure 1.- Pressure model of the supersonic aircraft configuration tested in the Langley 4- by 4-foot supersonic tunnel.

CONTENTS



CONFIDENTIAL

Figure 2.- Details of model of supersonic aircraft configuration. Dimensions are in inches unless otherwise noted.

CONFIDENTIAL

CONFIDENTIAL

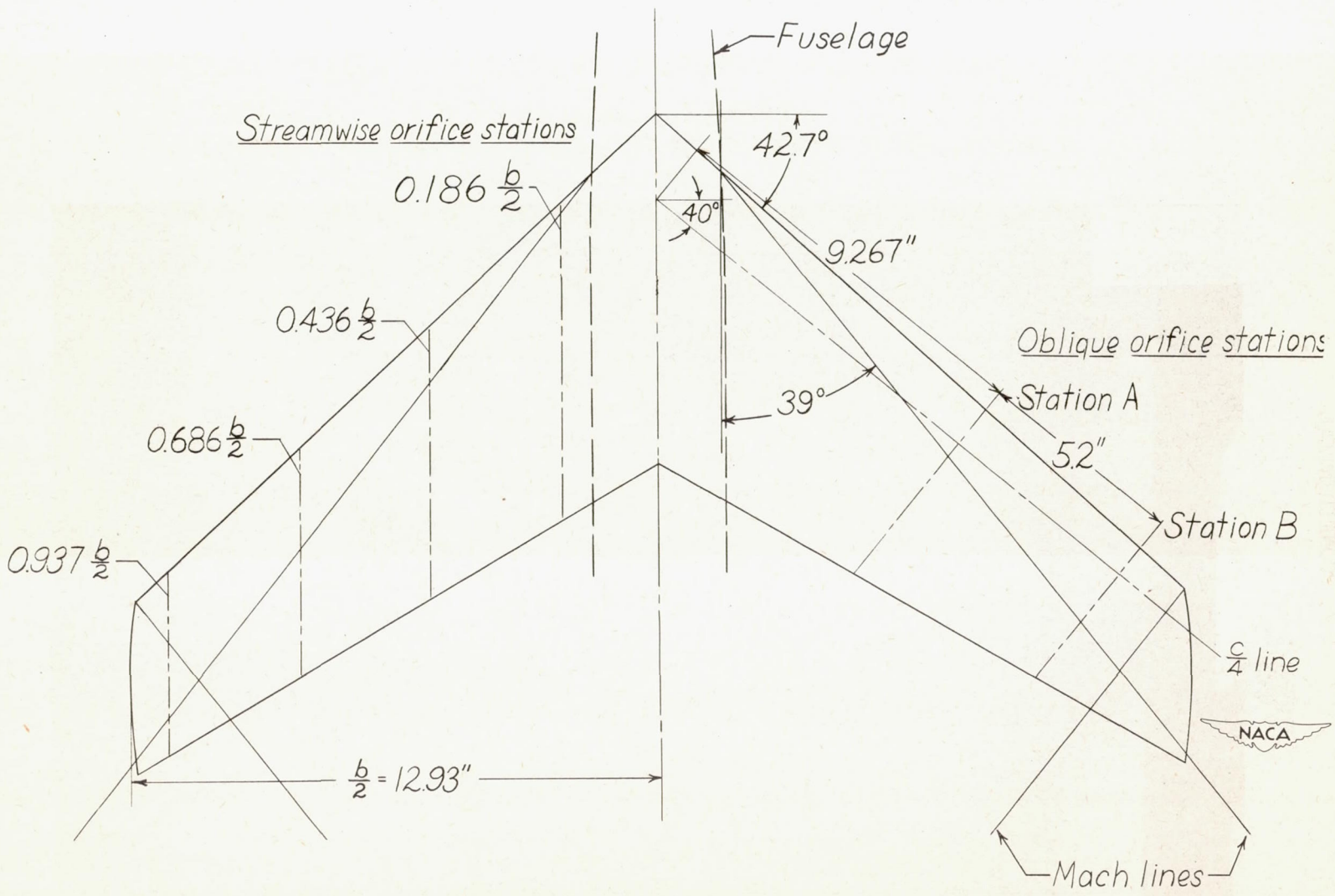


Figure 3.- Schematic view of wing showing orifice stations and Mach lines.

CONFIDENTIAL

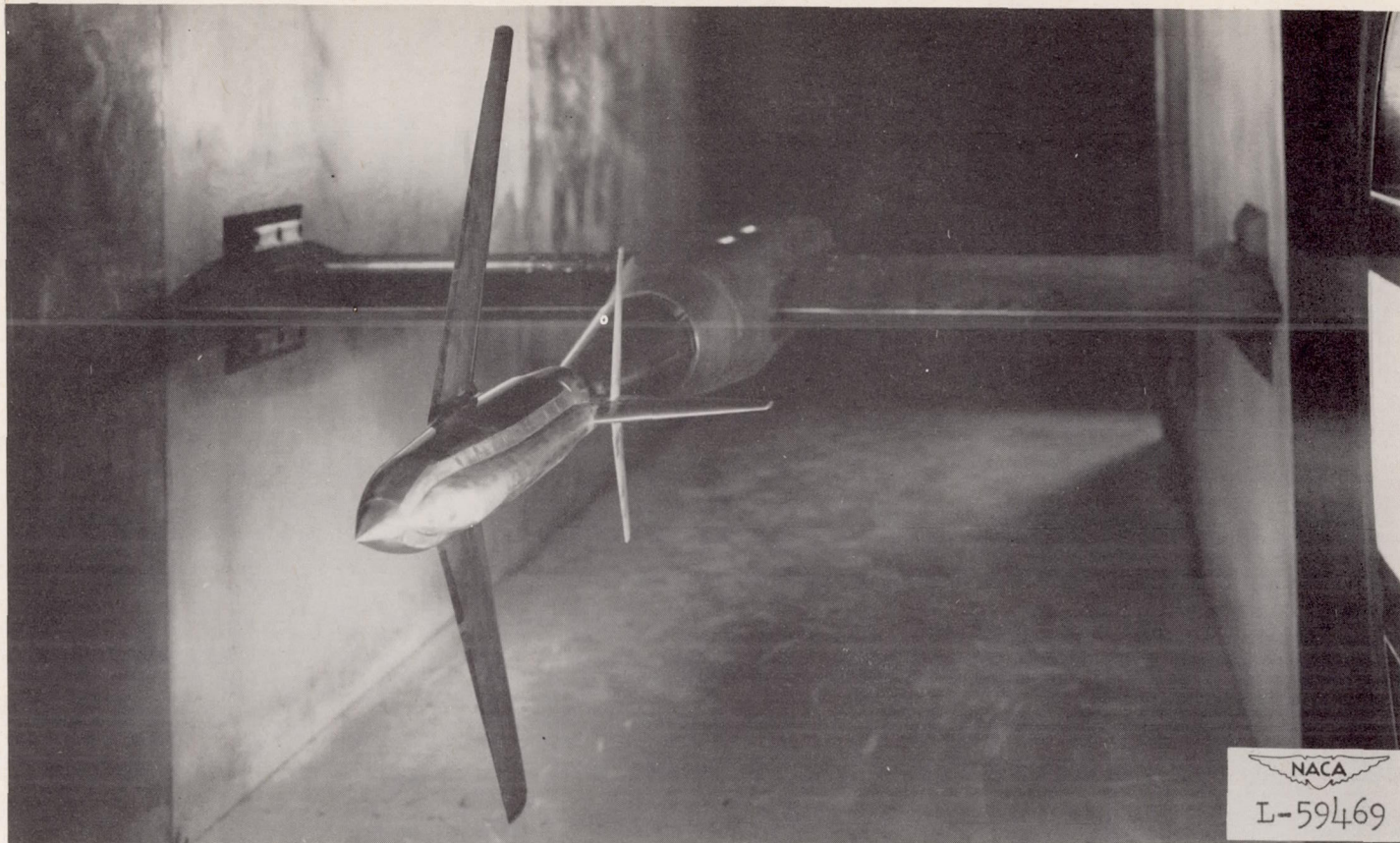
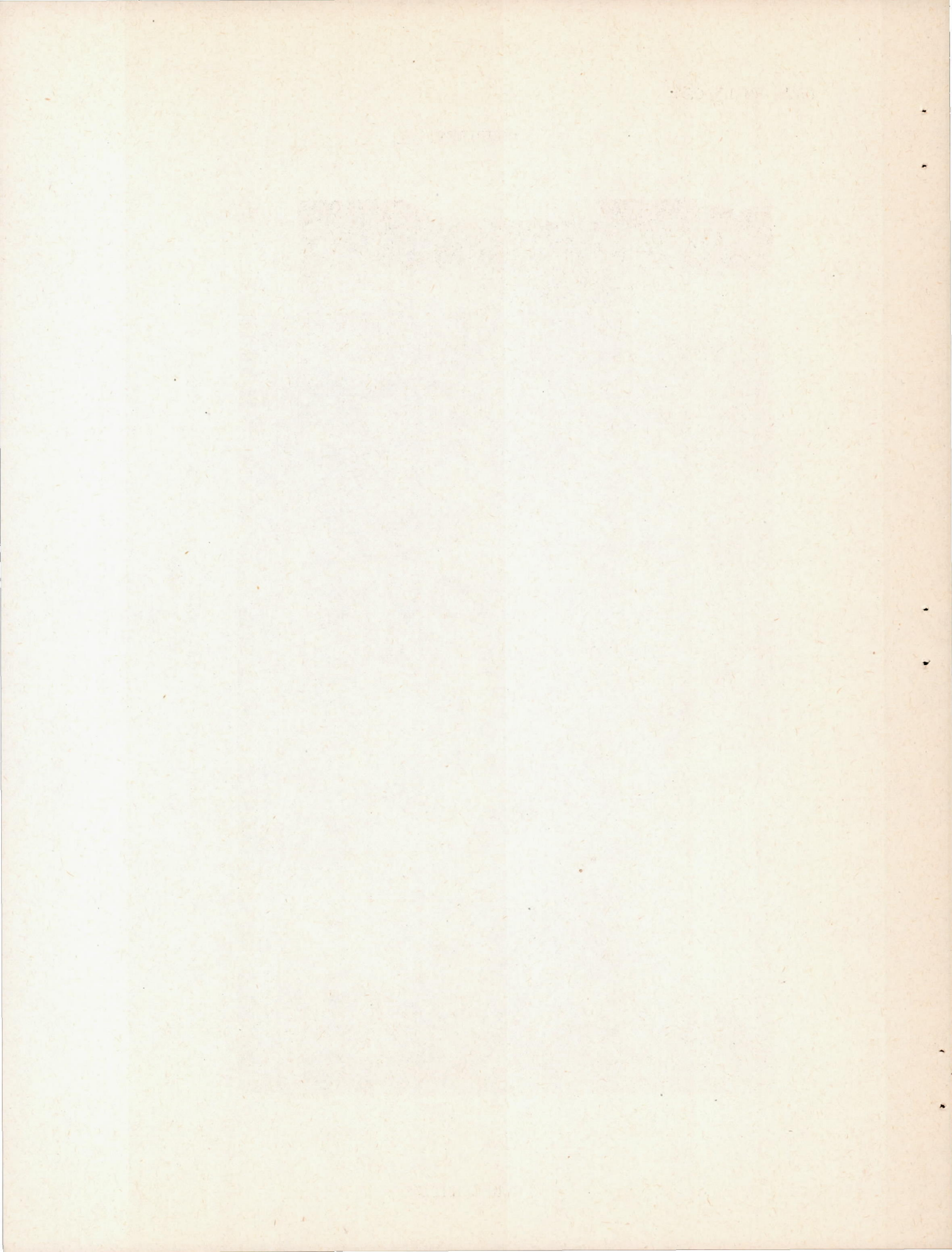
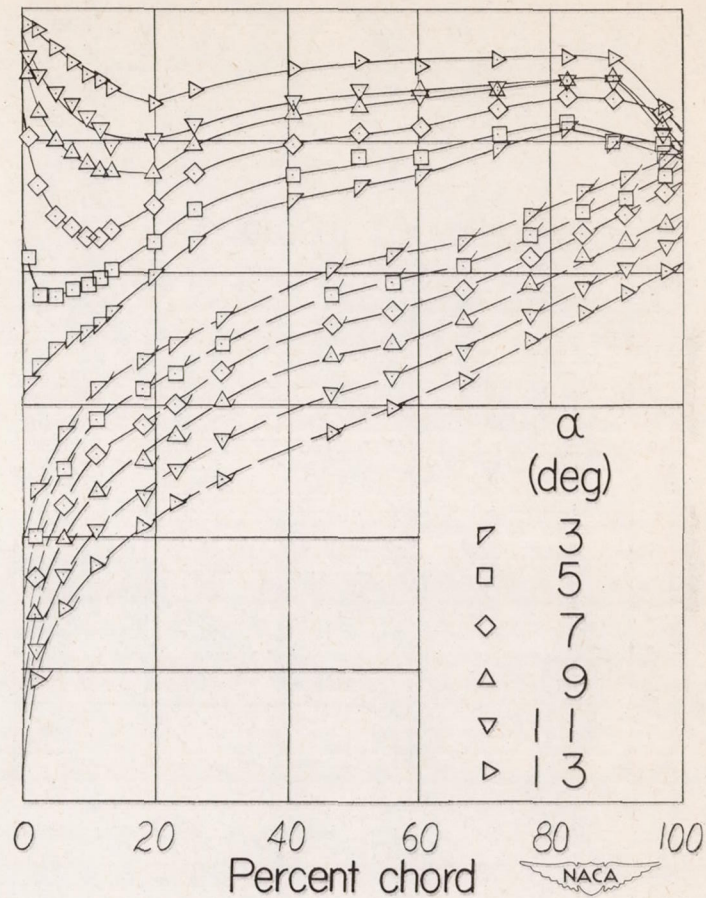
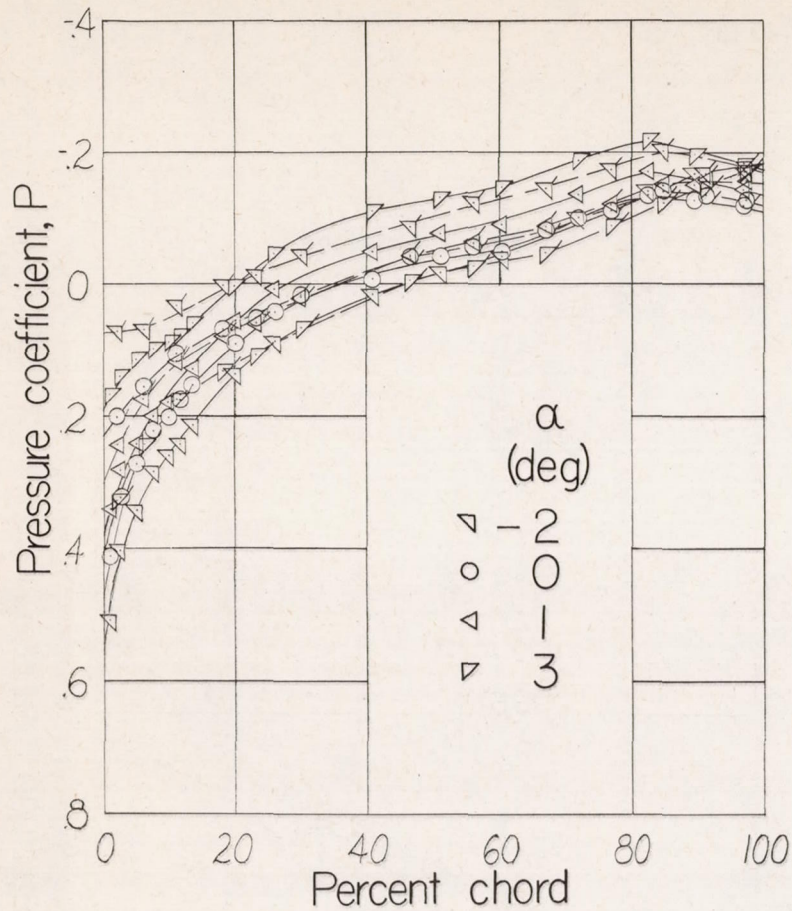


Figure 4.- Downstream view of test model mounted in the Langley 4-
by 4-foot supersonic tunnel.

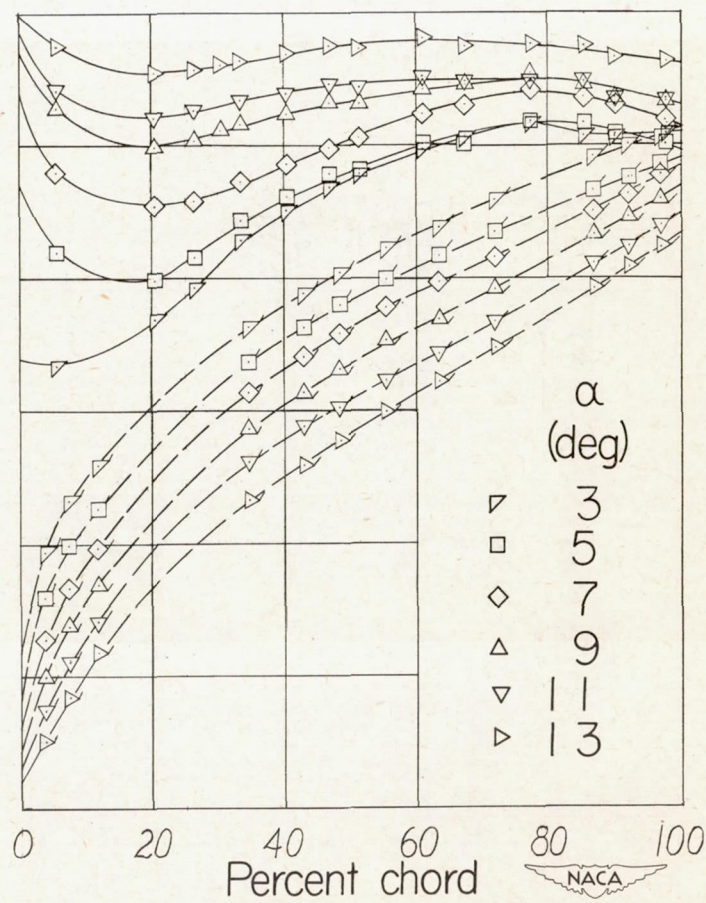
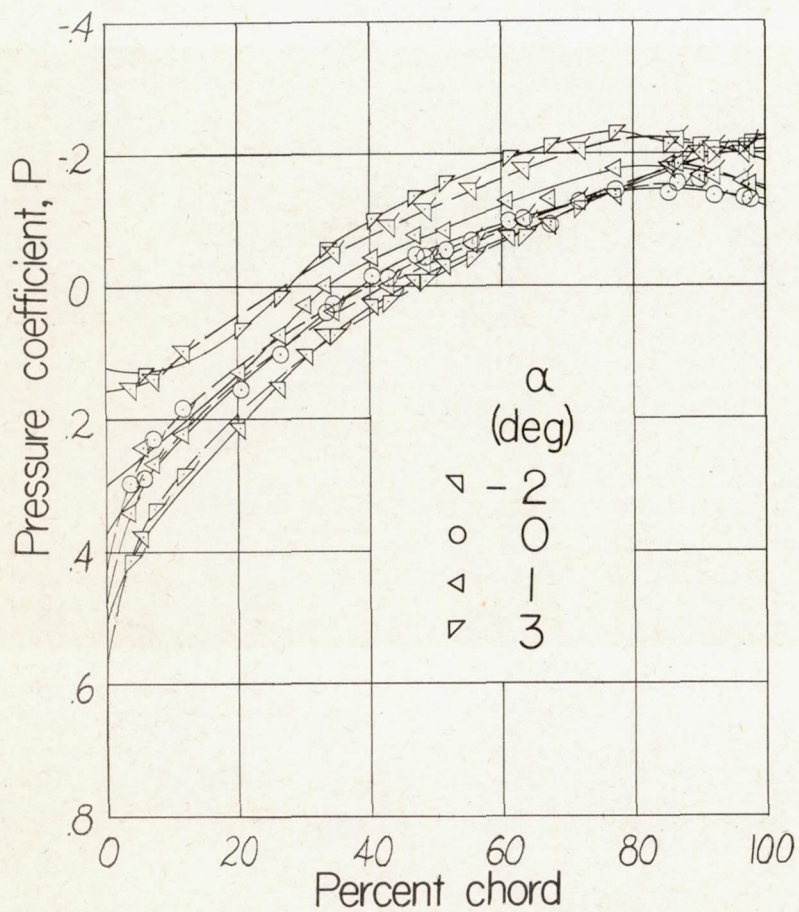
CONFIDENTIAL





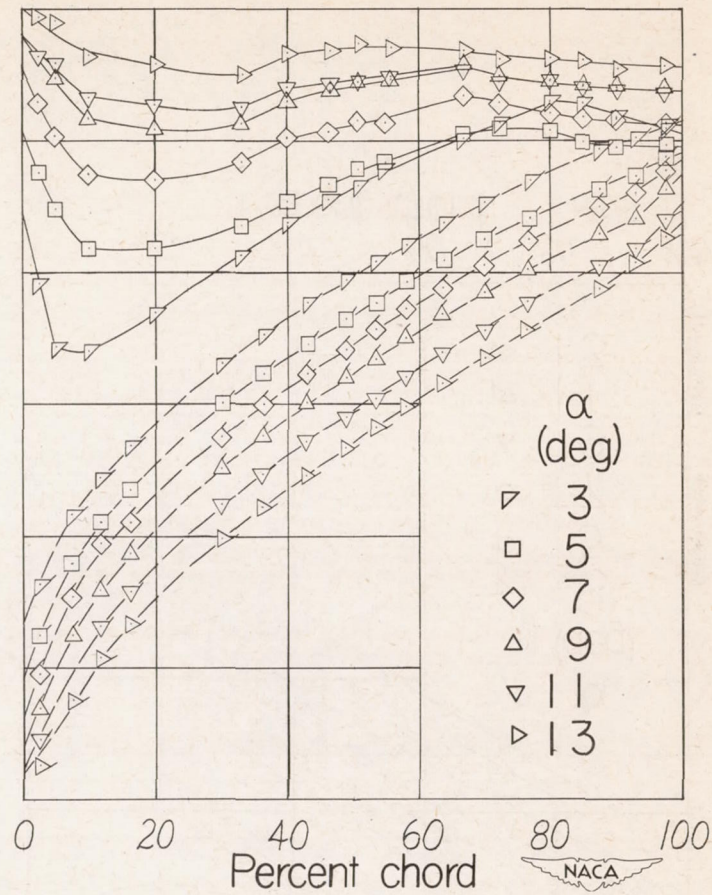
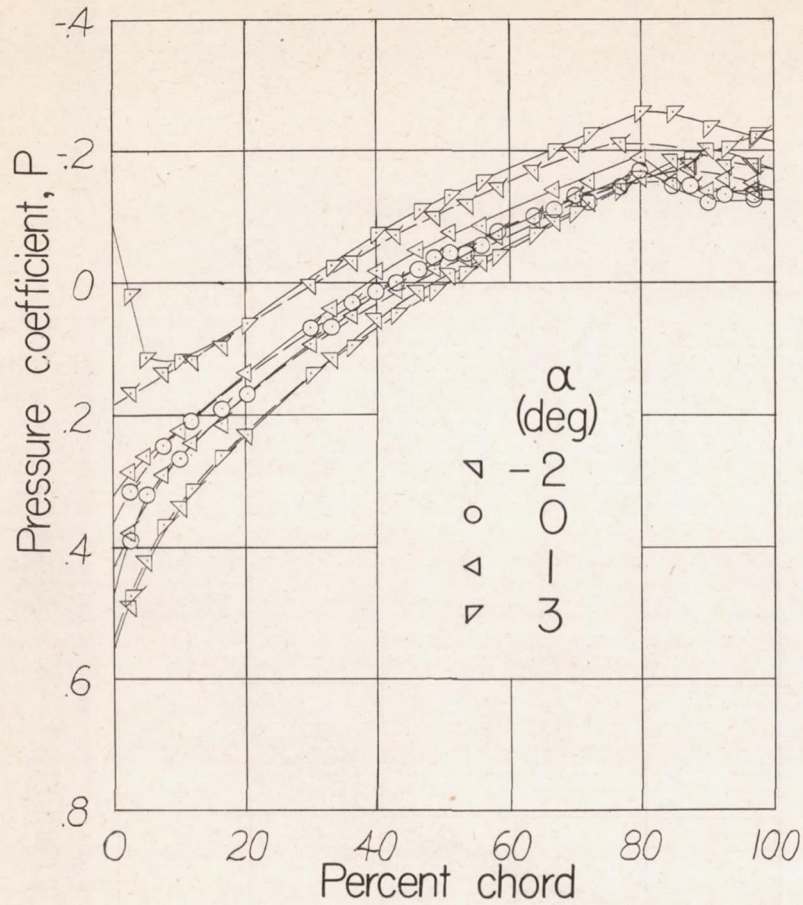
(a) $\frac{y}{b/2} = 0.186.$

Figure 5.- Variation of pressure distribution with angle of attack at four streamwise stations. Flagged symbols denote lower surface. $M = 1.59.$



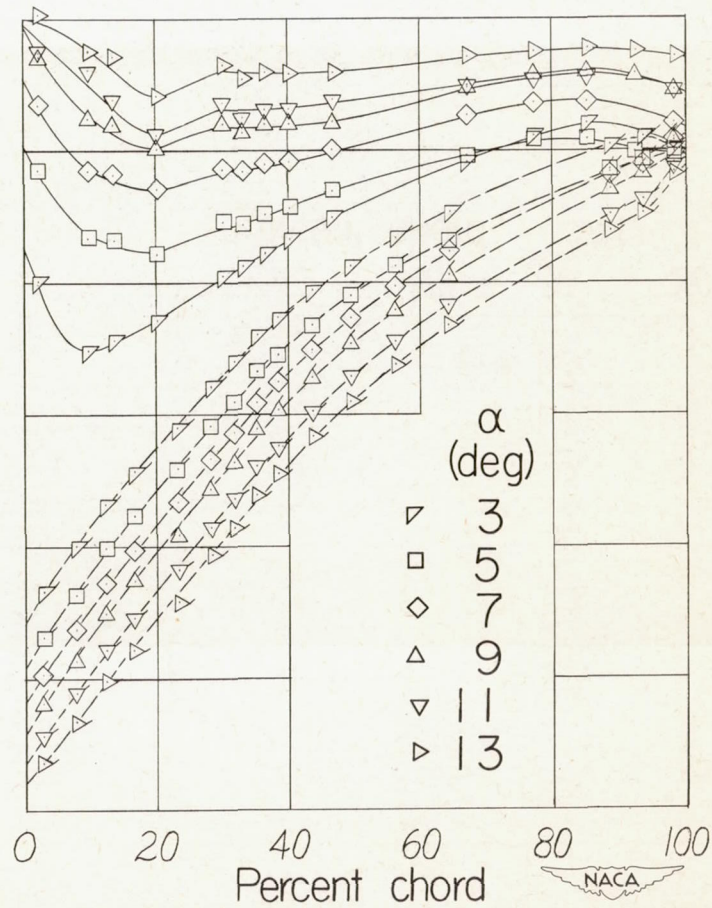
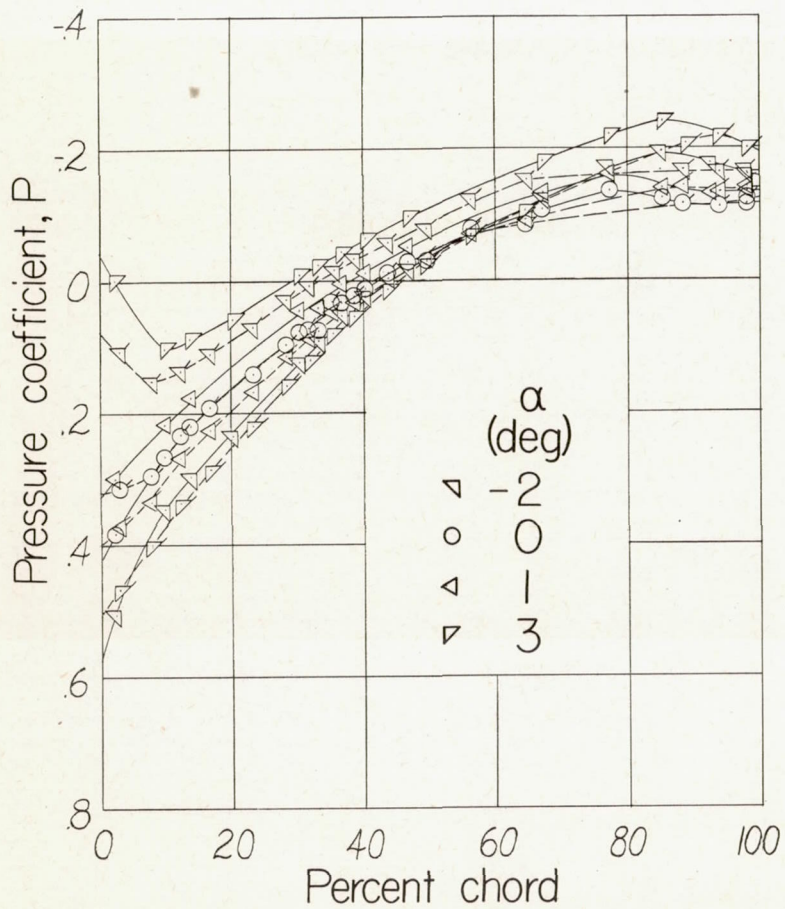
(b) $\frac{y}{b/2} = 0.436.$

Figure 5.- Continued.



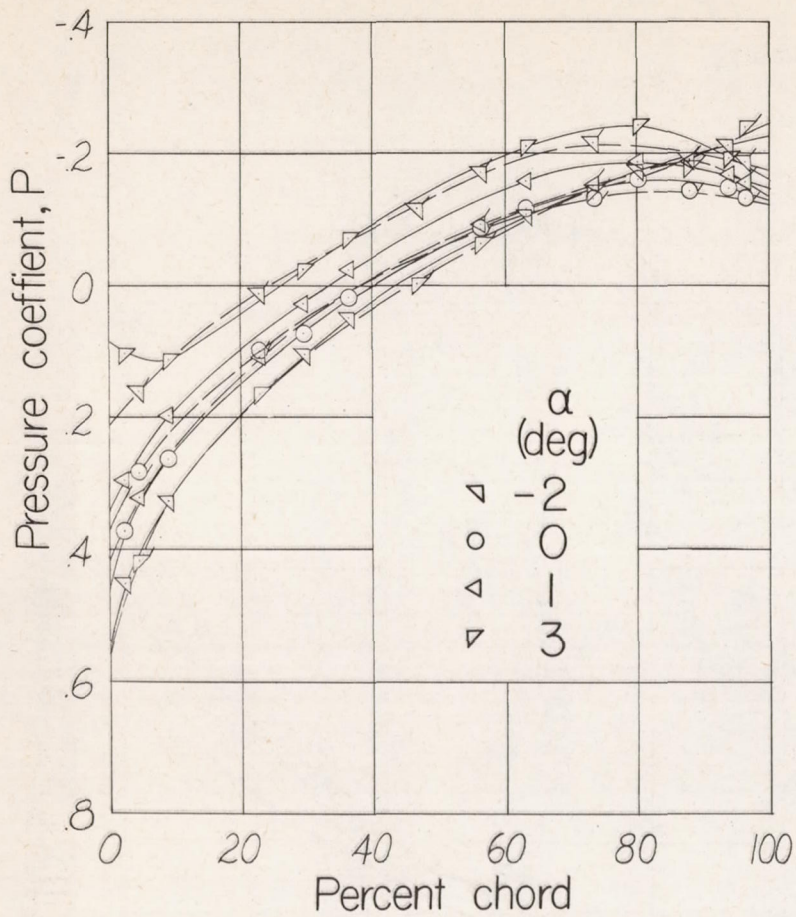
(c) $\frac{y}{b/2} = 0.686.$

Figure 5.- Continued.



(d) $\frac{y}{b/2} = 0.937.$

Figure 5.- Concluded.



(a) Station A.

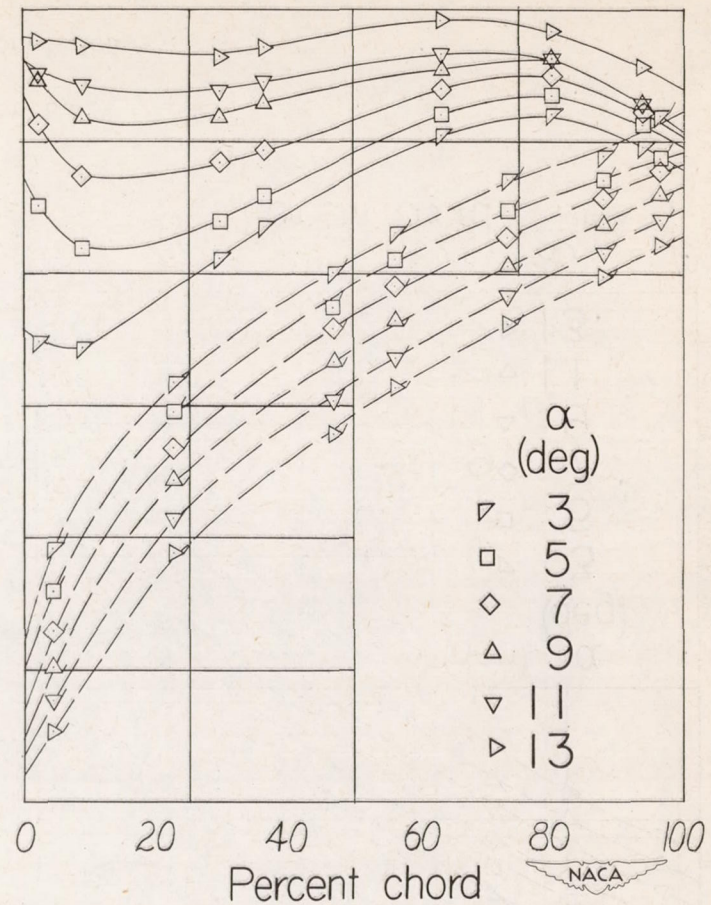
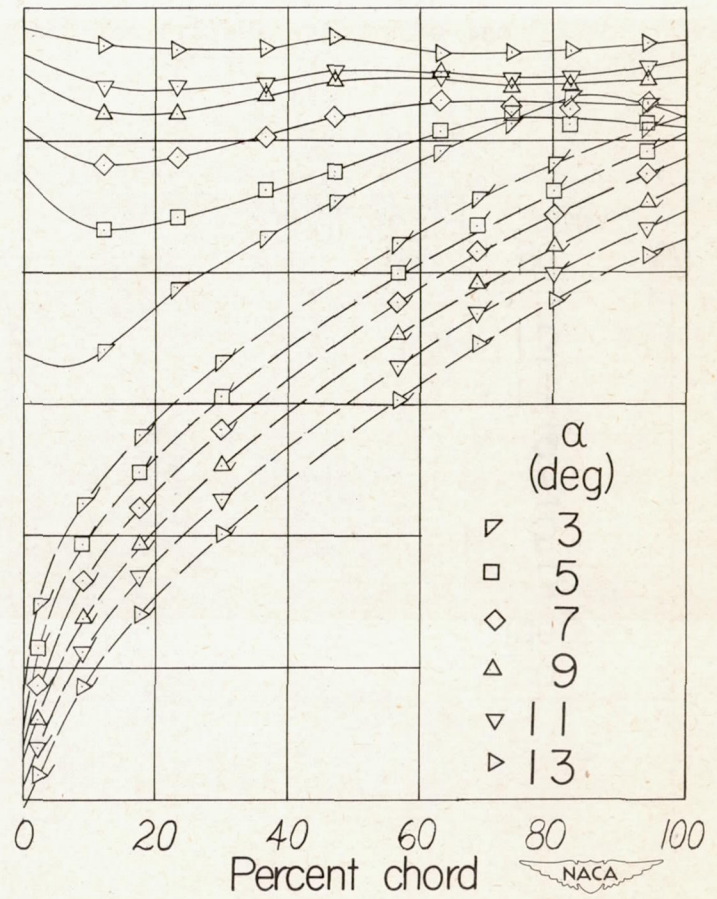
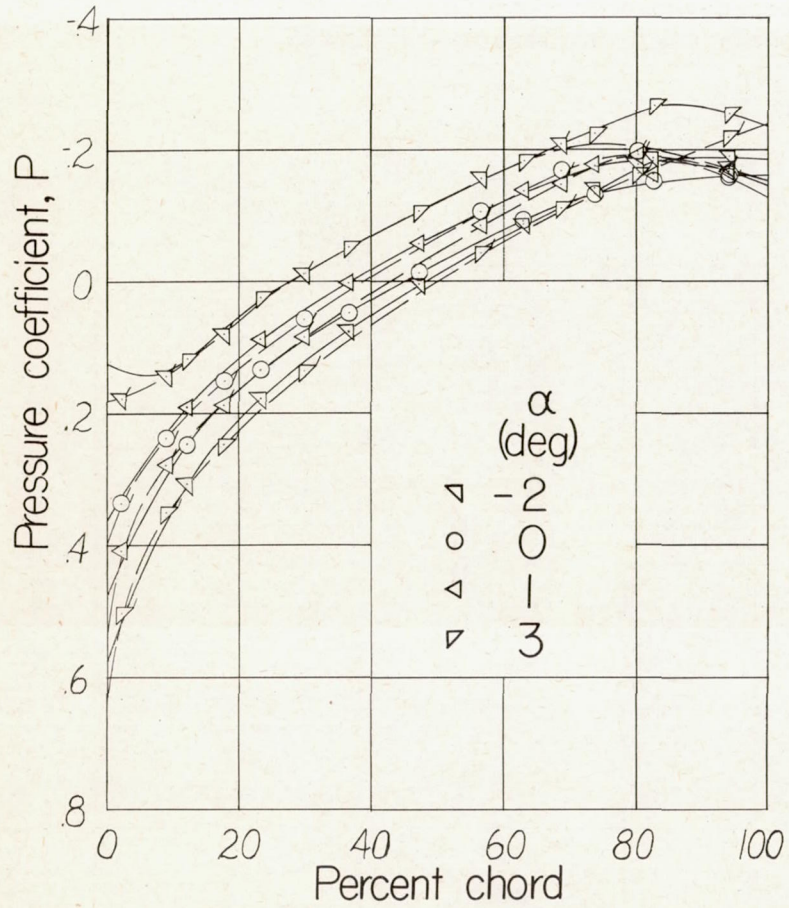
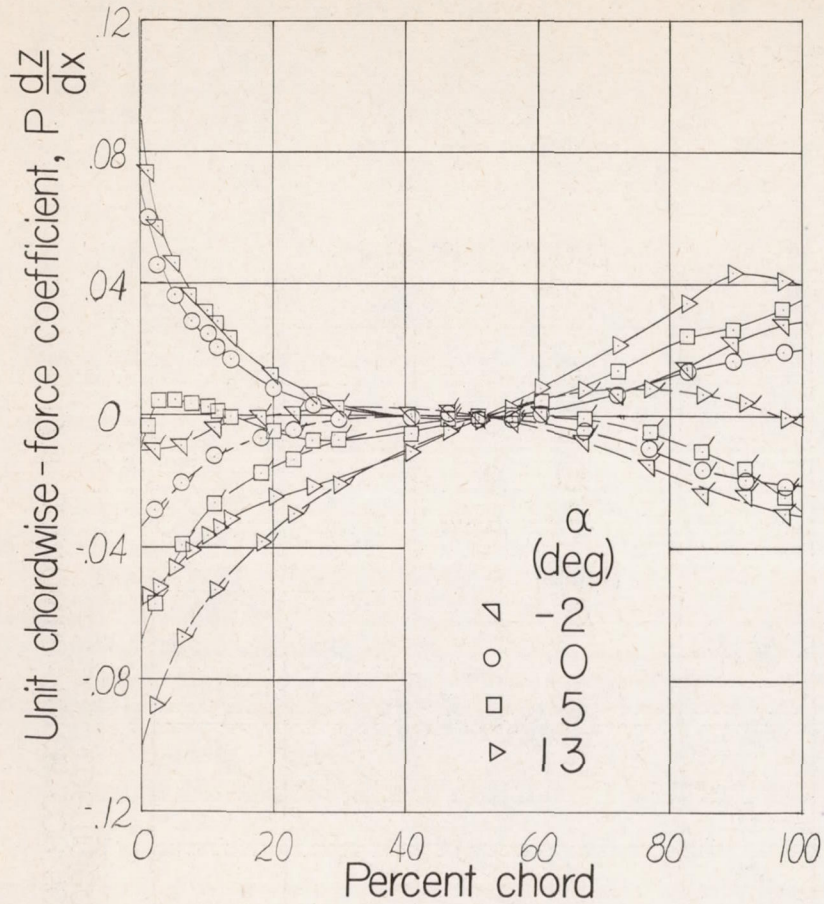


Figure 6.- Variation of pressure distribution with angle of attack at two oblique stations. Flagged symbols denote lower surface. $M = 1.59$.

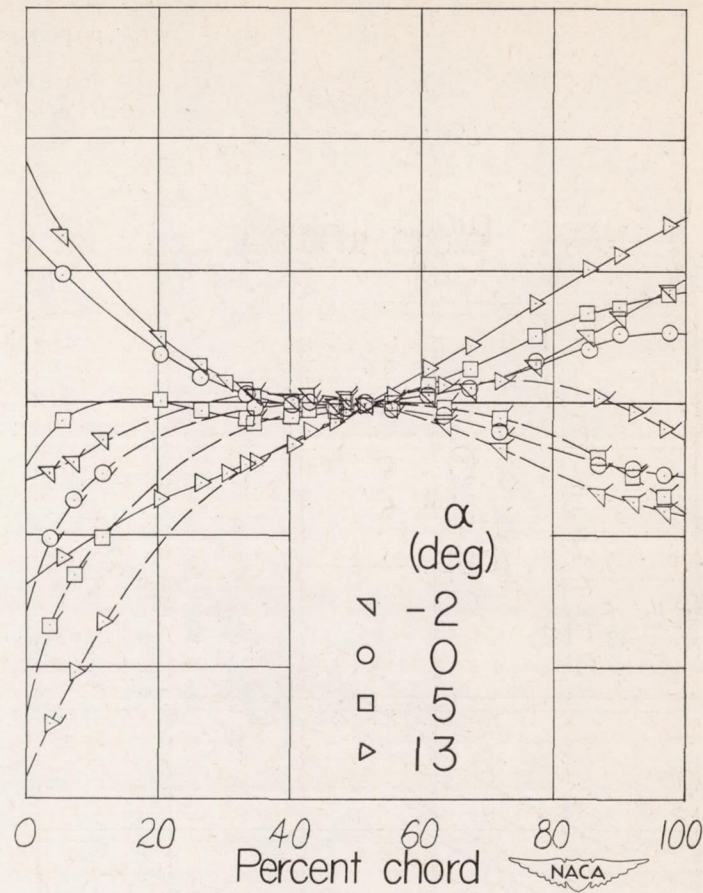


(b) Station B.

Figure 6.- Concluded.

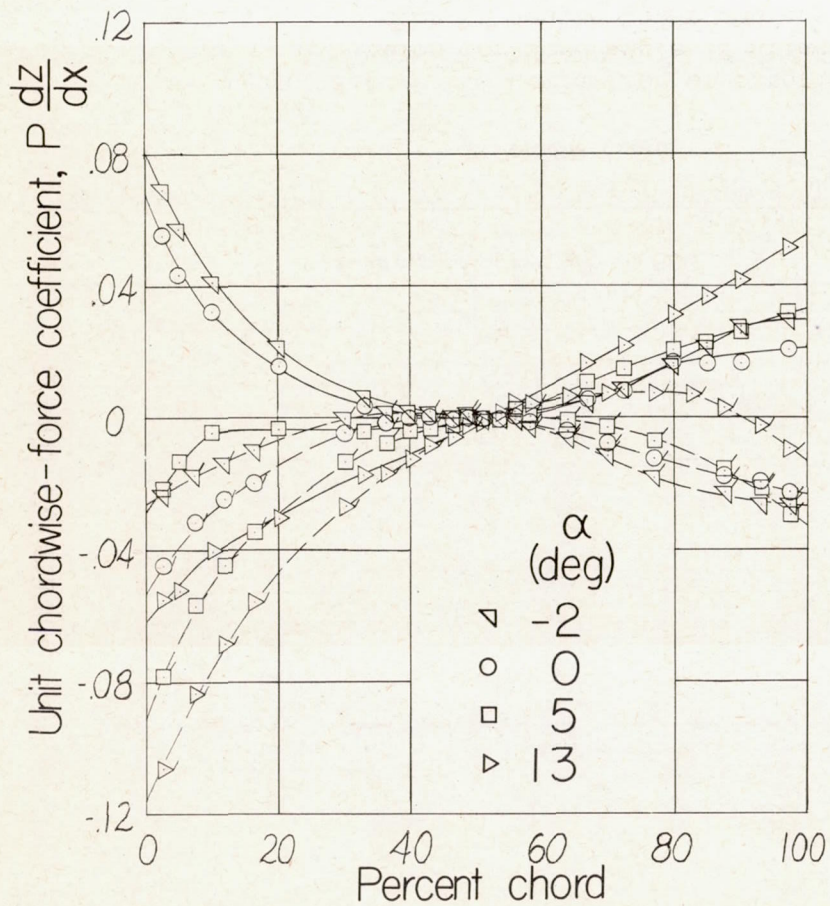


(a) $\frac{y}{b/2} = 0.186.$

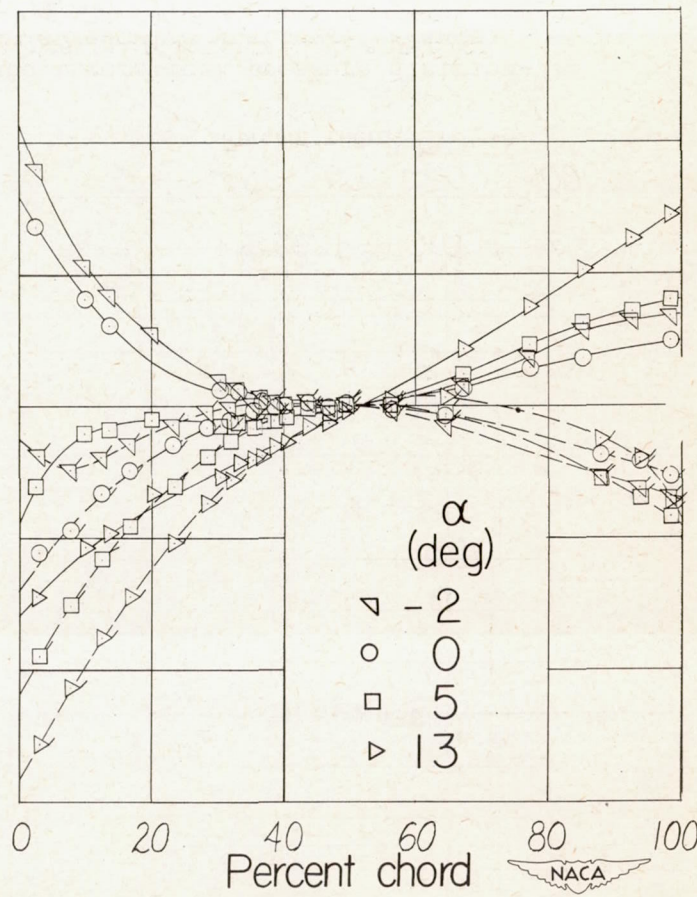


(b) $\frac{y}{b/2} = 0.436.$

Figure 7.- Variation of unit chordwise-force coefficient with angle of attack at four streamwise stations. Flagged symbols denote lower surface. $M = 1.59.$



(c) $\frac{y}{b/2} = 0.686.$



(d) $\frac{y}{b/2} = 0.937.$

Figure 7.- Concluded.

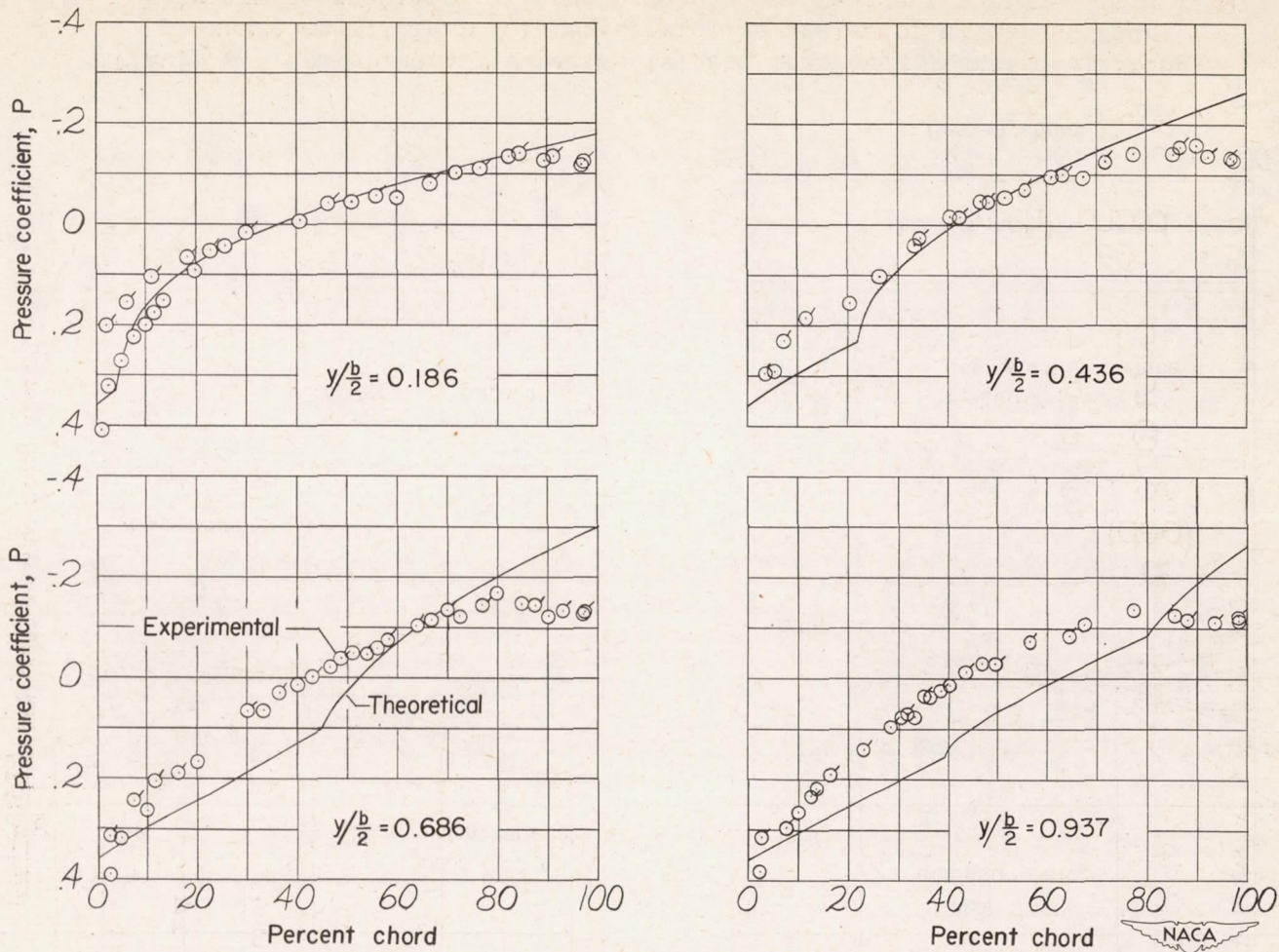


Figure 8.- Comparison of experimental and theoretical pressure distribution for zero angle of attack at four streamwise stations. Flagged symbols denote lower surface. $M = 1.59$.

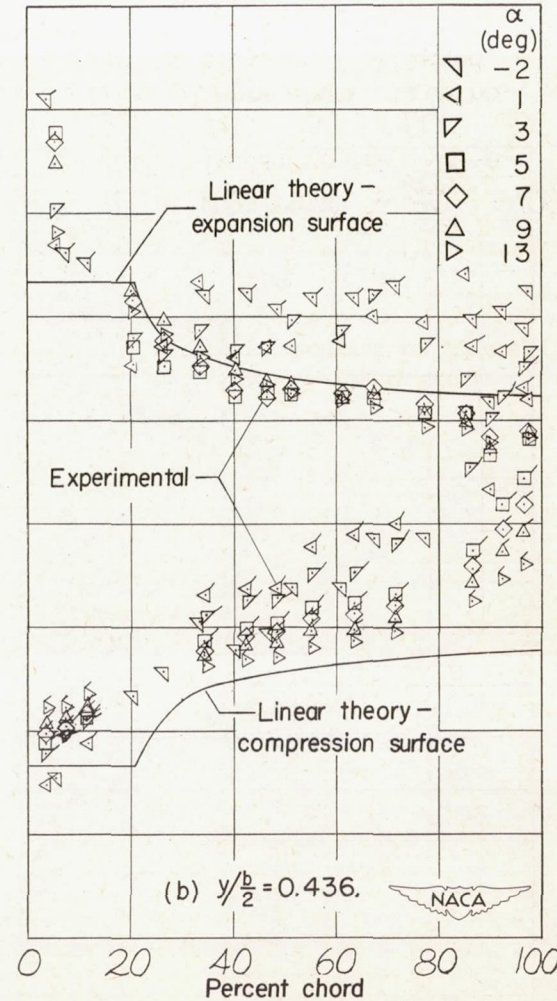
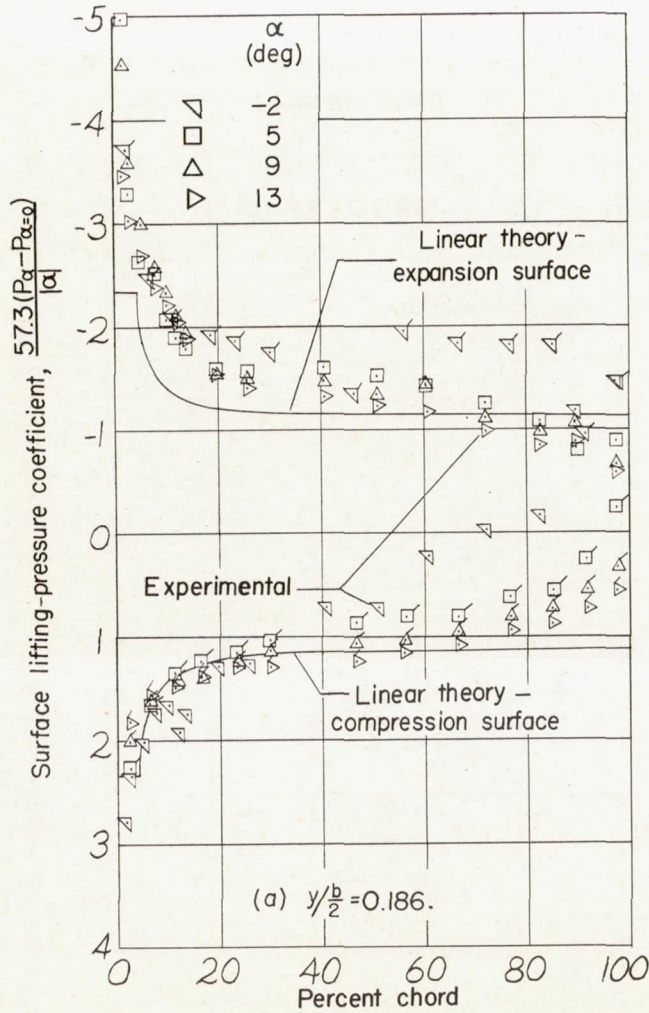


Figure 9.- Comparison of experimental and theoretical surface lifting-pressure coefficient for representative angles of attack at four streamwise stations. Flagged symbols denote lower surface. $M = 1.59$.

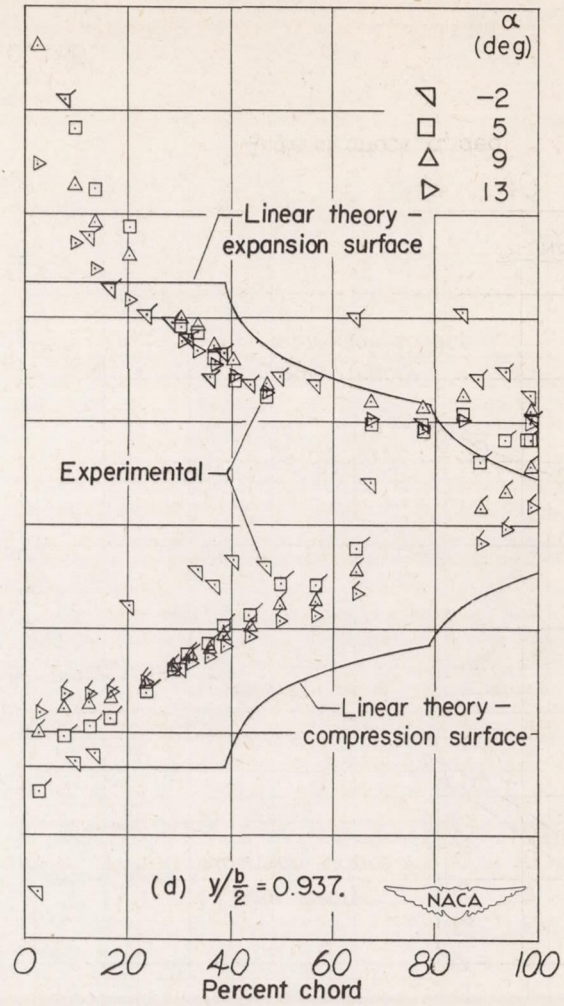
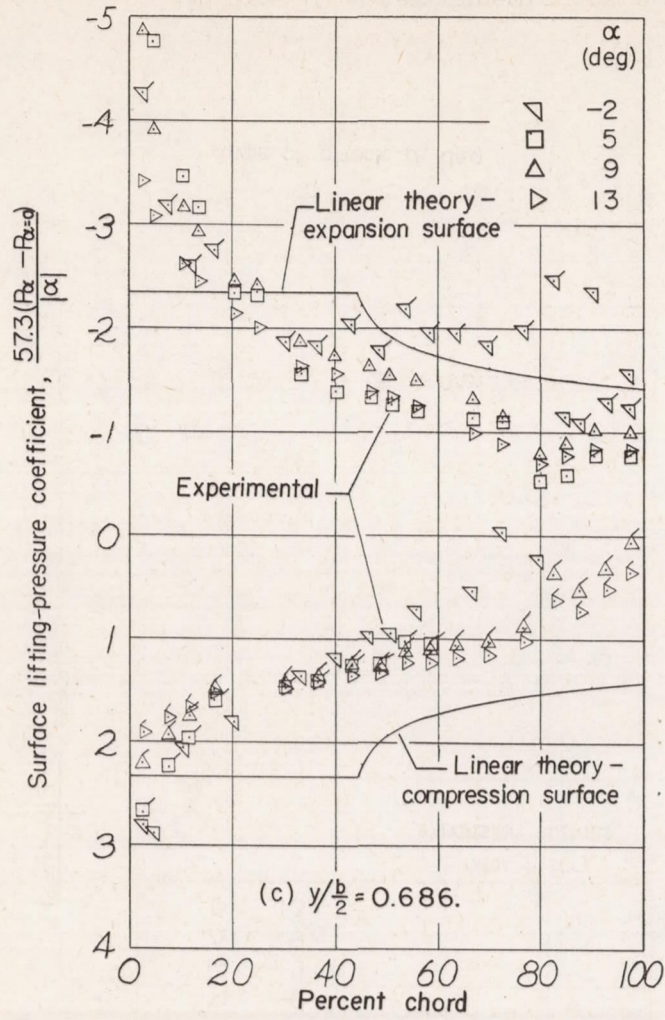
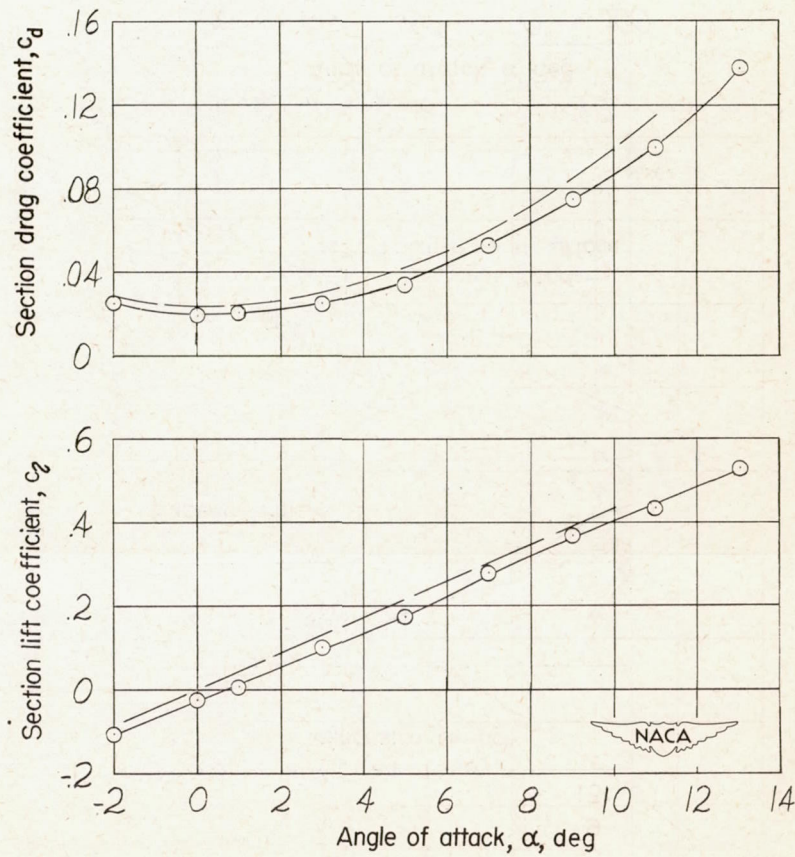
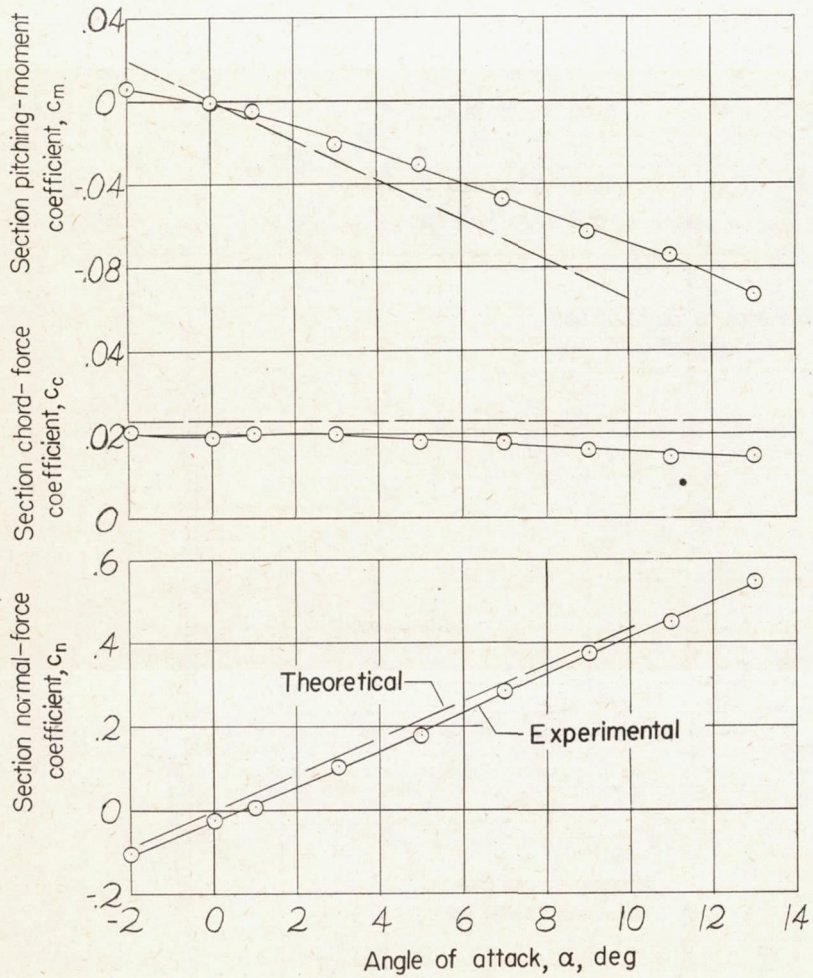
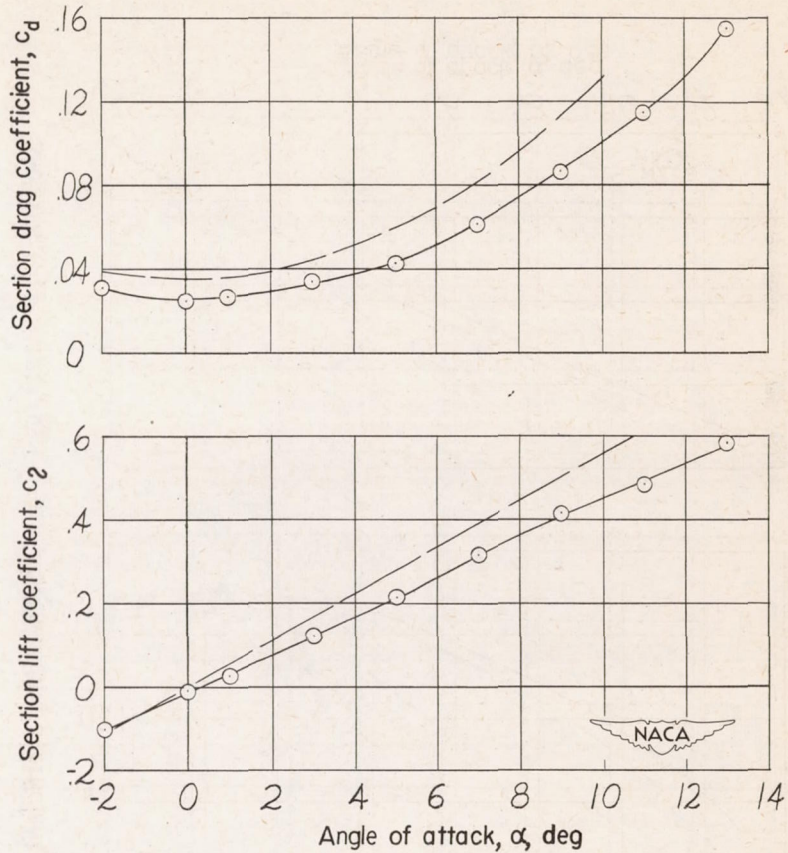
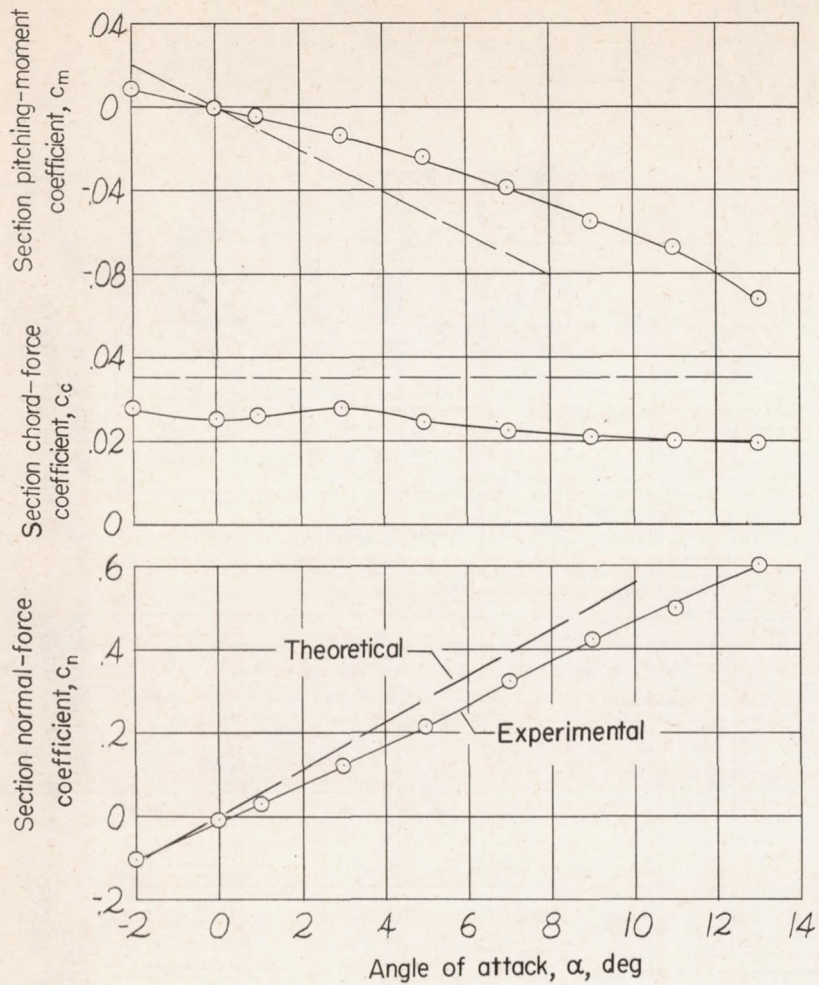


Figure 9.- Concluded.



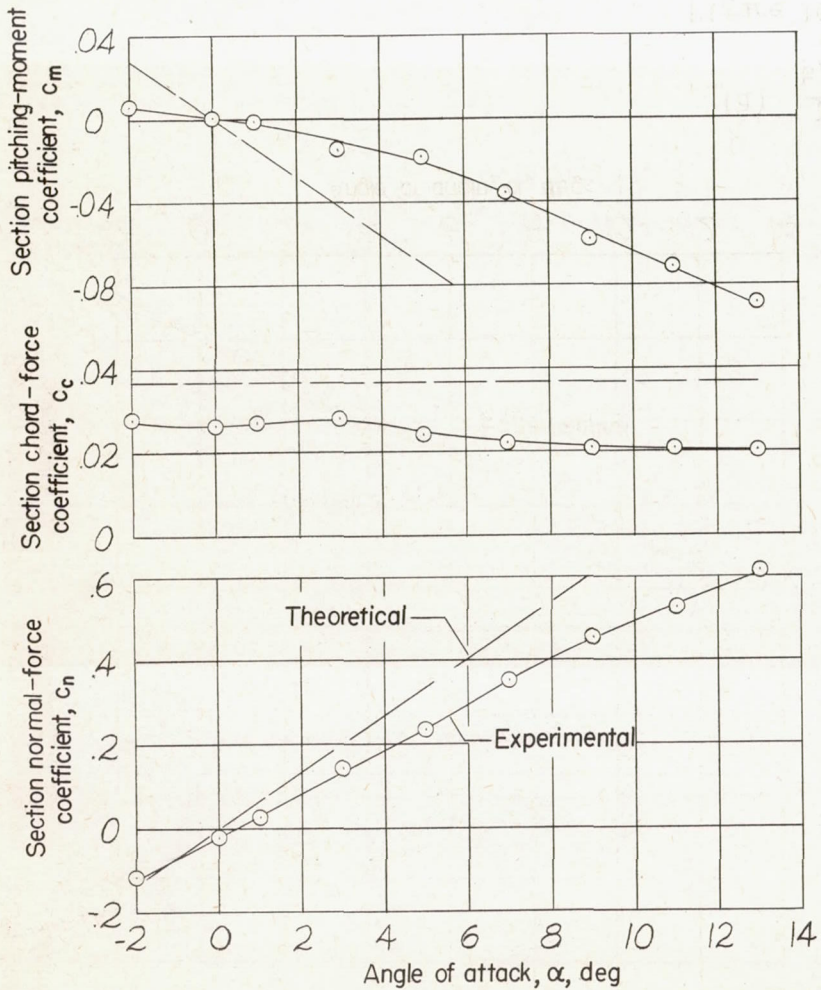
(a) $\frac{y}{b/2} = 0.186.$

Figure 10.- Aerodynamic characteristics at four streamwise stations.
 $M = 1.59.$



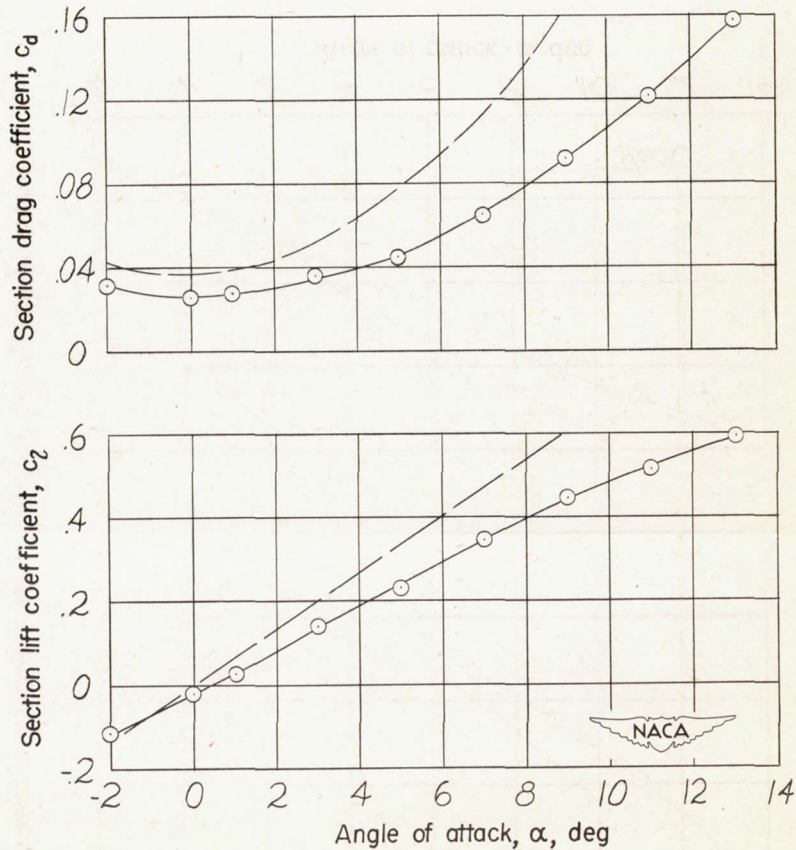
(b) $\frac{y}{b/2} = 0.436.$

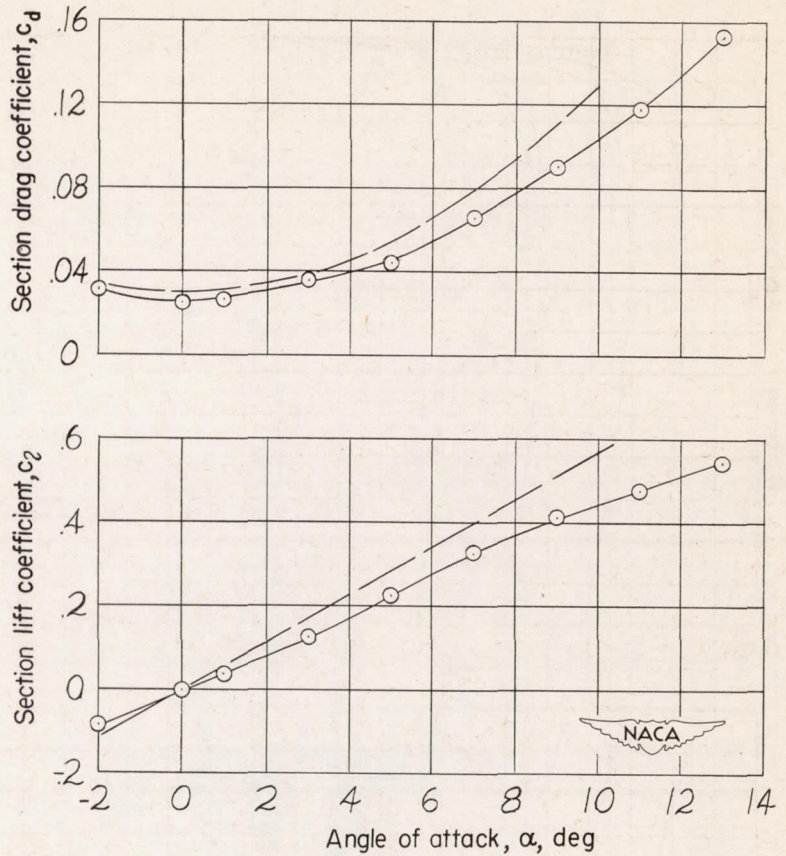
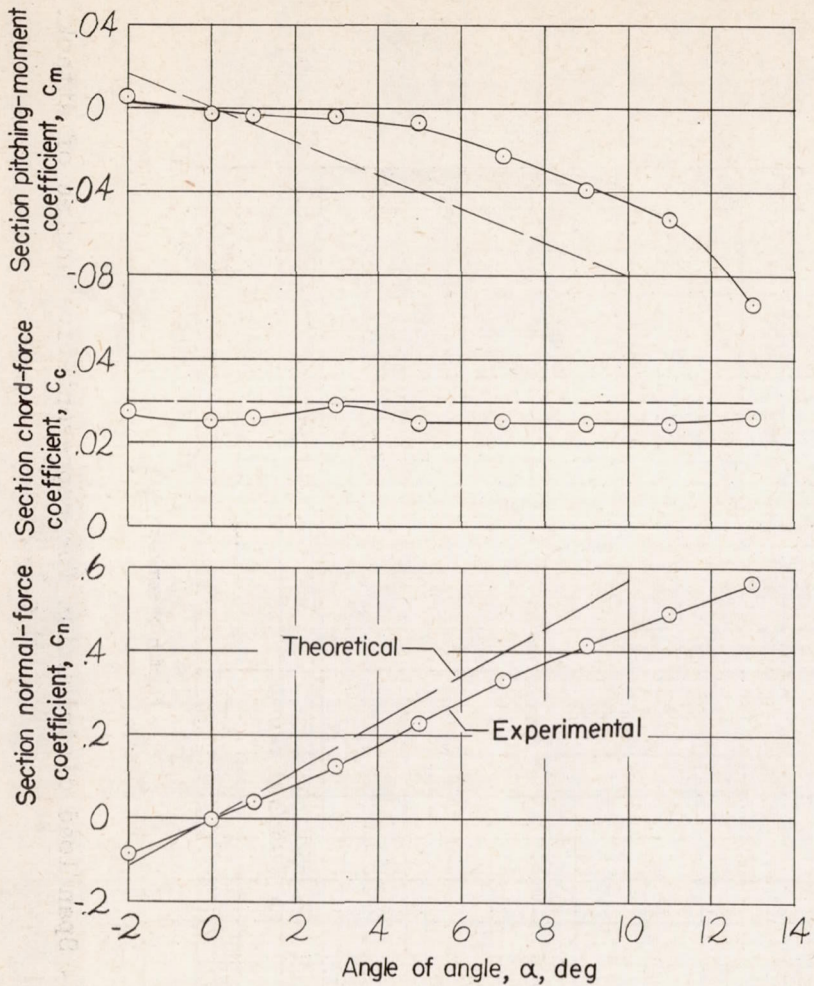
Figure 10.- Continued.



(c) $\frac{y}{b/2} = 0.686.$

Figure 10.- Continued.





(d) $\frac{y}{b/2} = 0.937.$

Figure 10.- Concluded.

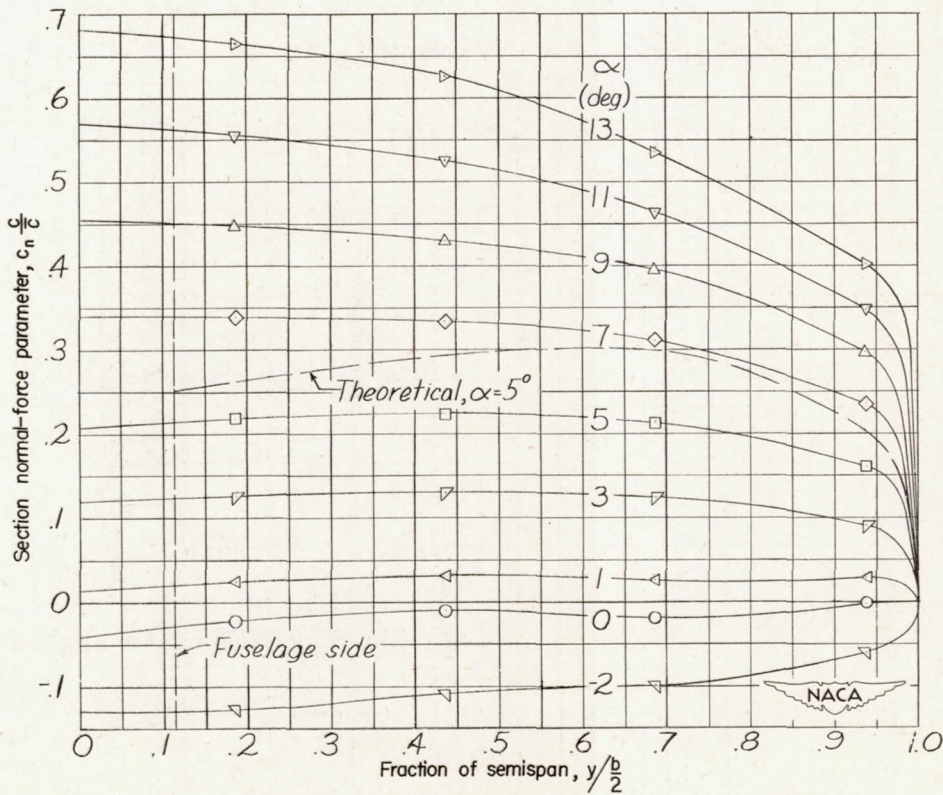
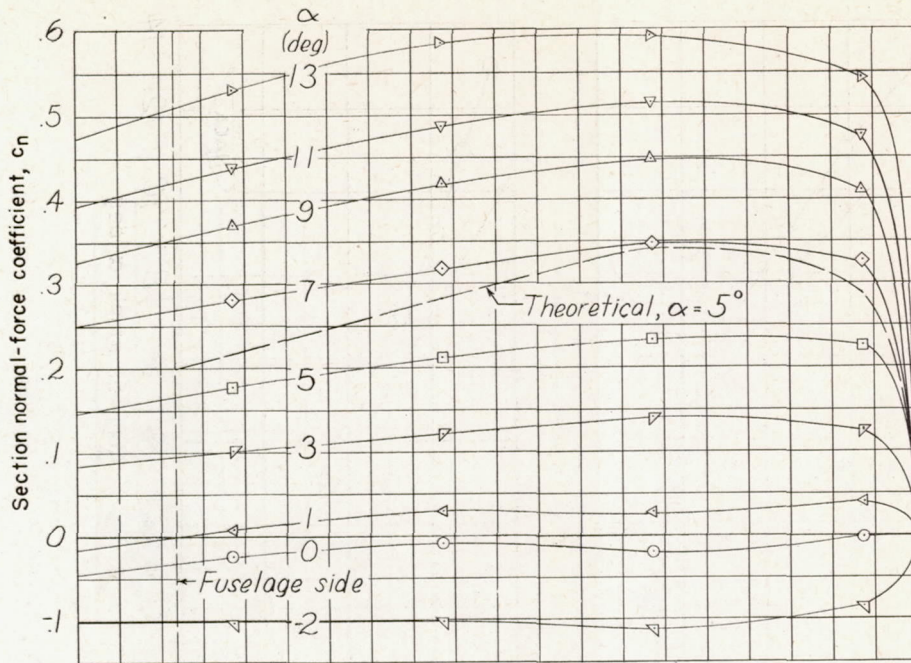


Figure 11.- Span load distribution for representative angles of attack.
 M = 1.59.

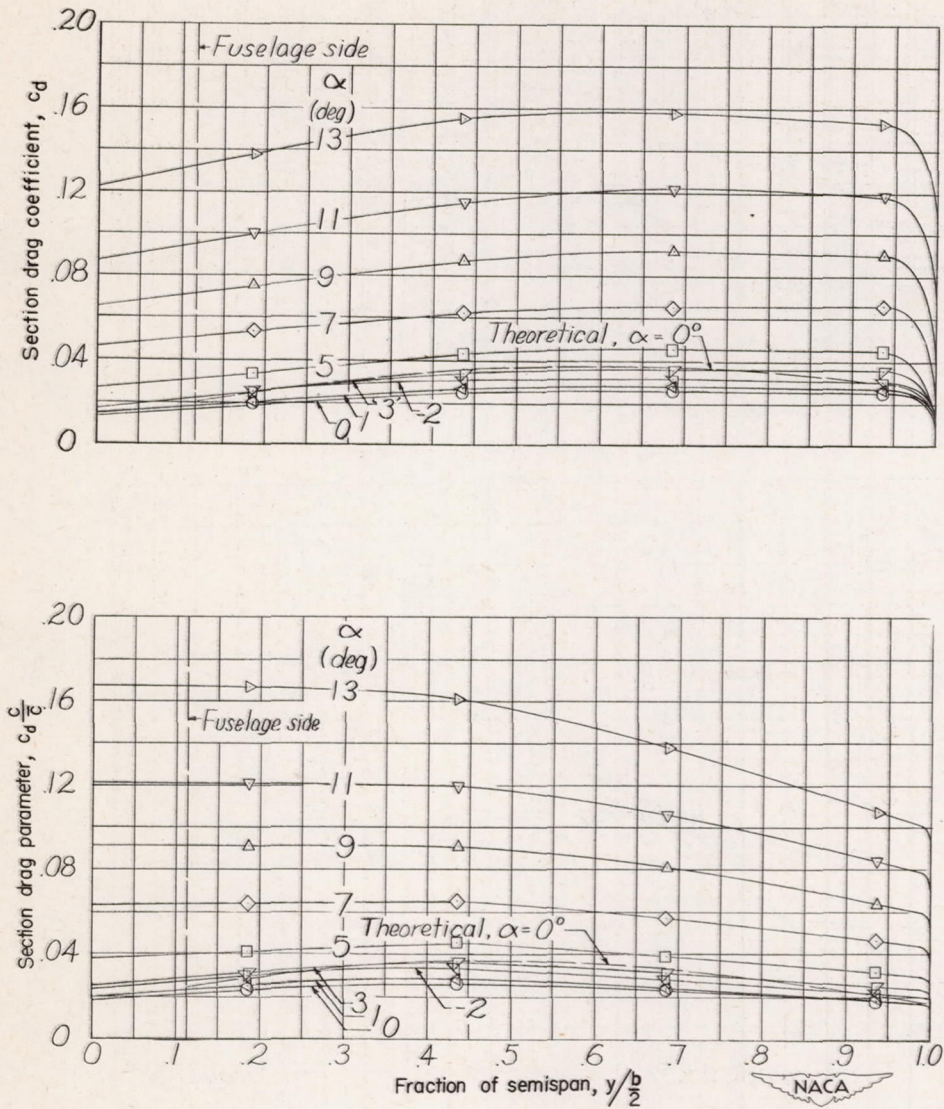


Figure 12.- Spanwise distribution of drag for representative angles of attack. $M = 1.59$.

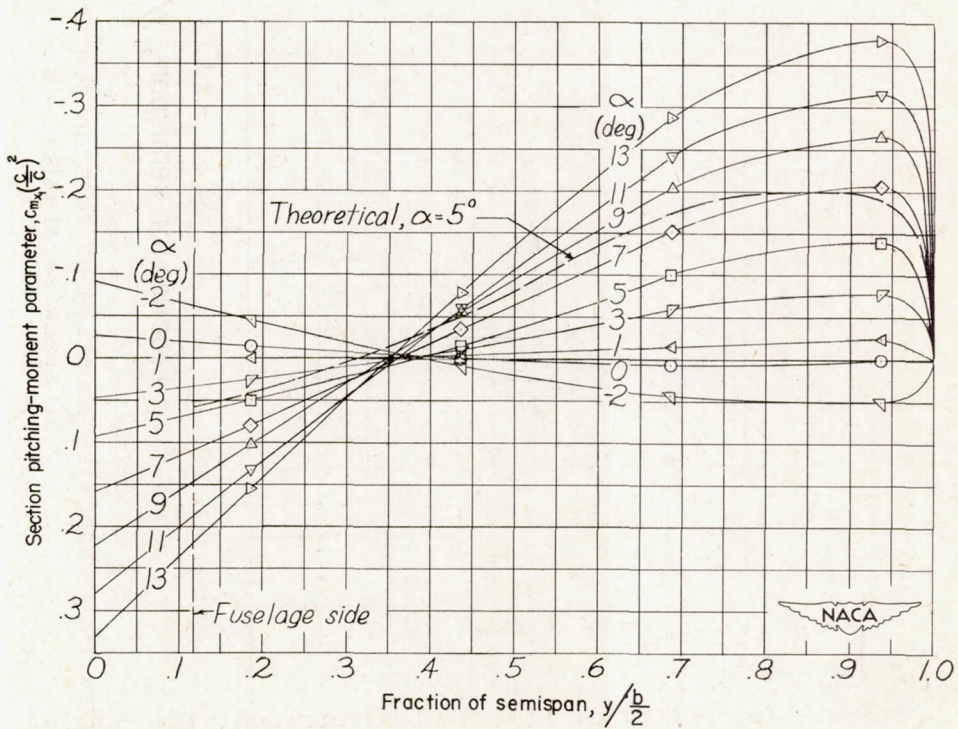
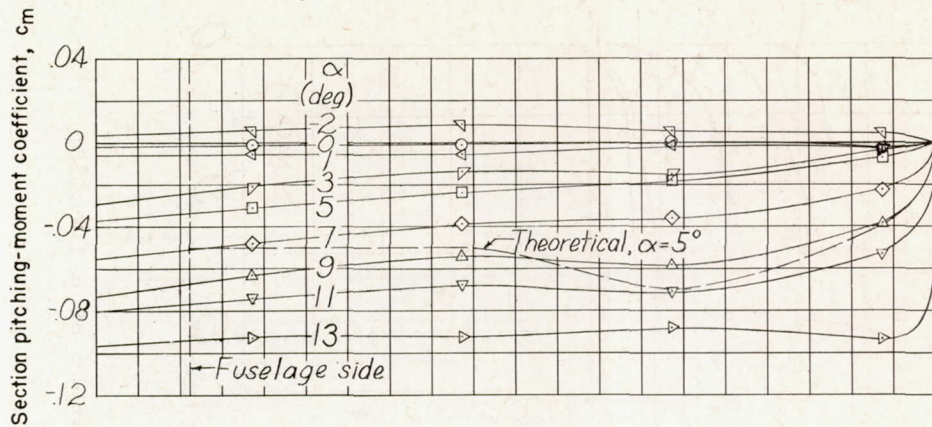


Figure 13.- Spanwise distribution of pitching-moment for representative angles of attack. $M = 1.59$.

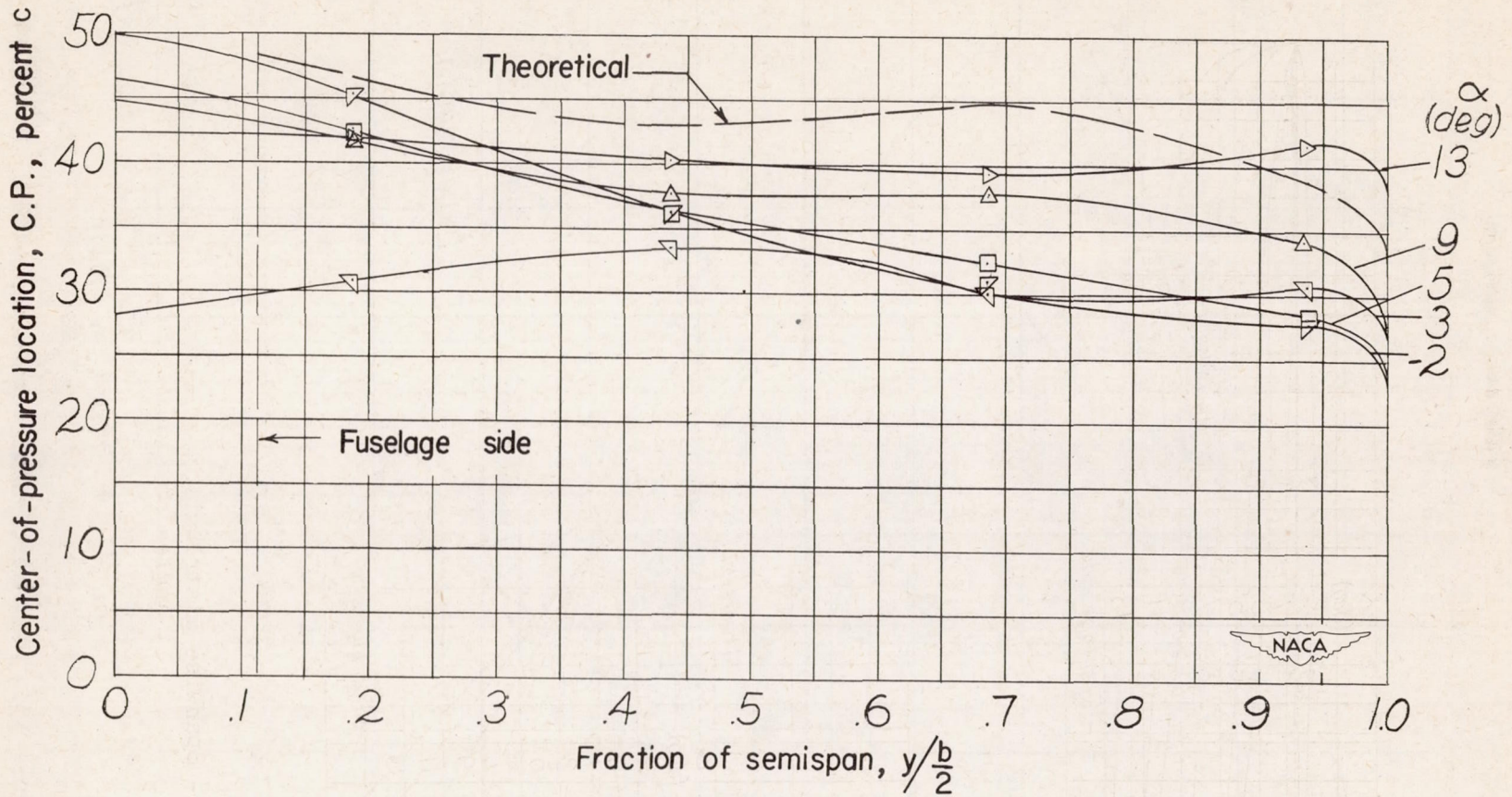


Figure 14.- Chordwise location of section center of pressure as a function of spanwise station. $M = 1.59$.

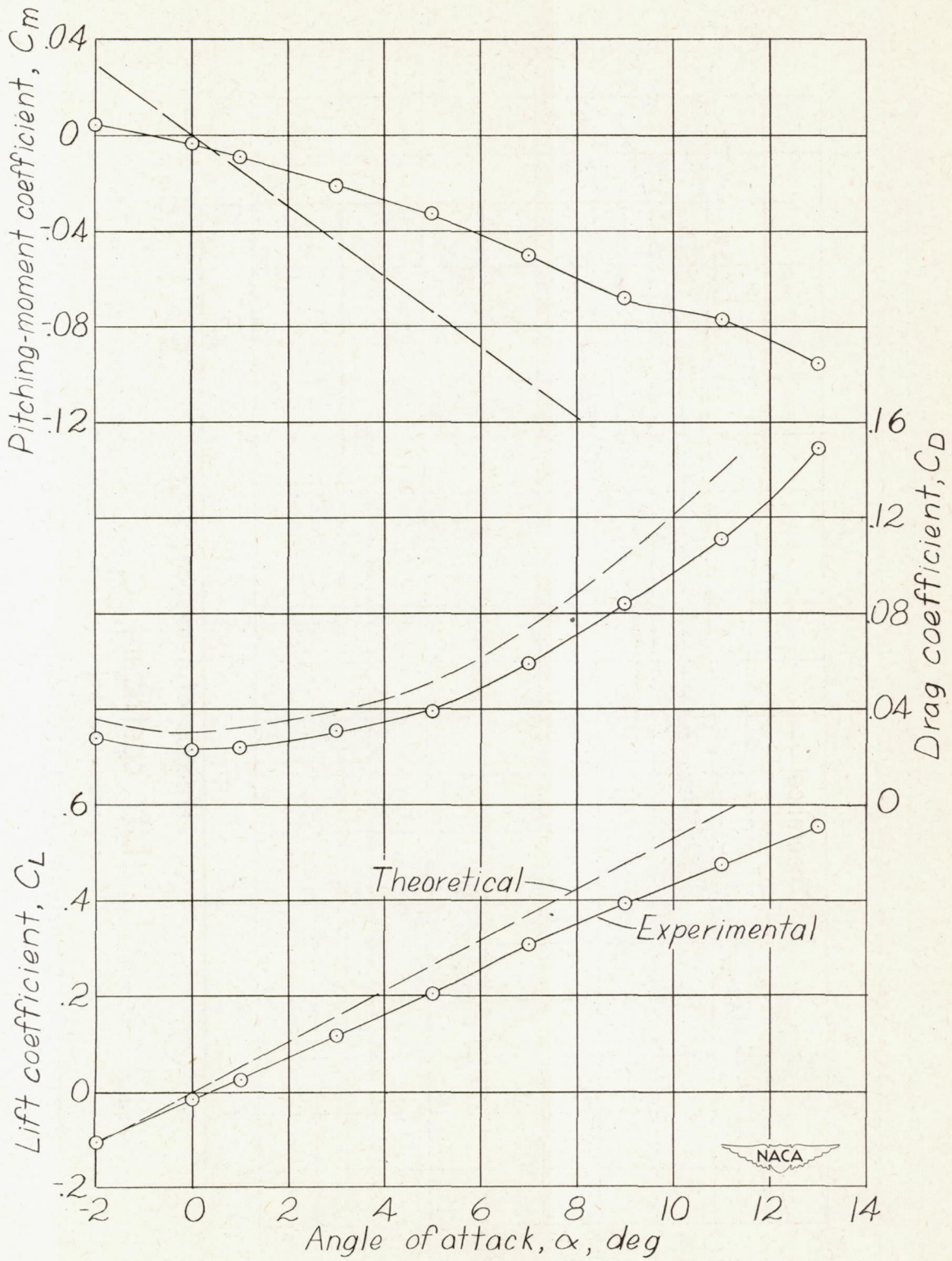


Figure 15.- Wing aerodynamic characteristics. $M = 1.59$.

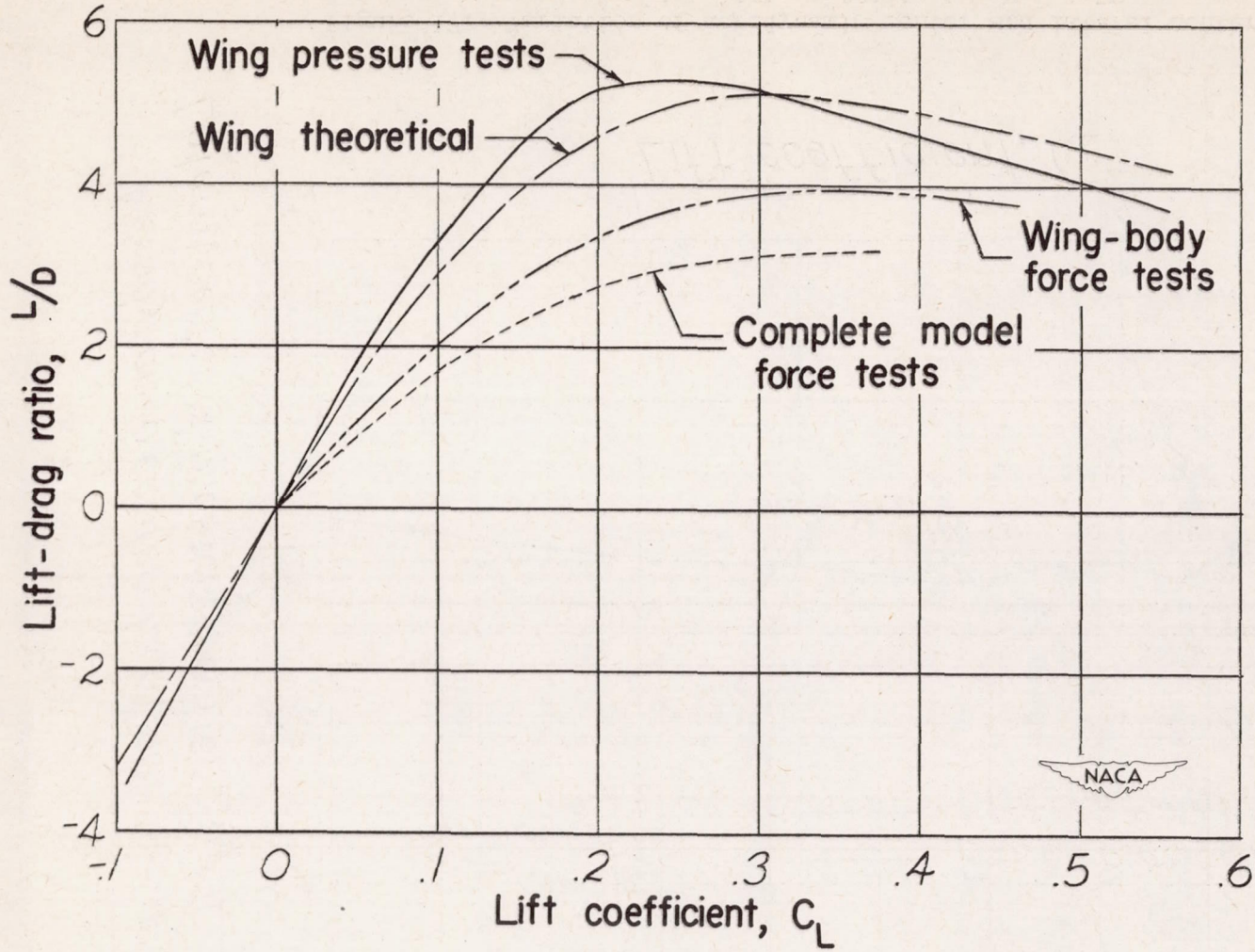


Figure 16.- Experimental and theoretical lift-drag ratios. $M = 1.59$.

Aerodynamic-center location, n_0 , percent c'
 Lateral center-of-pressure location, $y_{cp}/\frac{b}{2}$

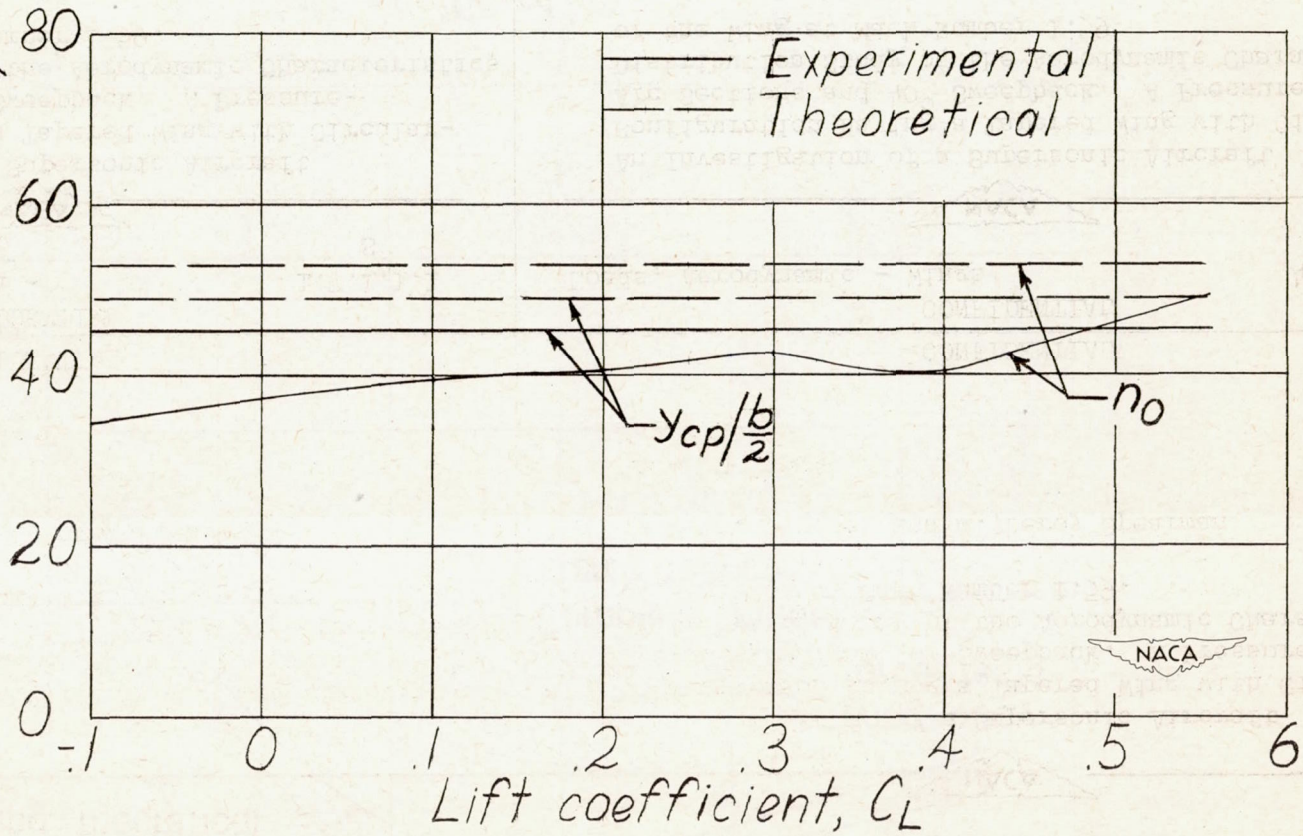


Figure 17.- Variation of aerodynamic center and lateral center of pressure with lift coefficient. $M = 1.59$.